Data-Driven Screening to Infer Metabolic Modulators of the Cancer Epigenome

Scott E. Campit[1], Rupa Bhowmick[2], Taoan Lu[3], Aaditi Vivek Saoji[3], Ran Jin[2,4], Aaron M. Robida[5], Sriram Chandrasekaran[1,2,6,]*

[1]Program in Chemical Biology, University of Michigan, Ann Arbor.
[2]Department of Biomedical Engineering, University of Michigan, Ann Arbor.
[3]Department of Electrical Engineering and Computer Science, University of Michigan, Ann Arbor.
[4]Department of Cellular and Molecular Biology, University of Michigan, Ann Arbor.
[5] Center for Chemical Genomics, University of Michigan, Ann Arbor.
[6]Rogel Cancer Center, University of Michigan Medical School, Ann Arbor, MI, 48109, USA.
* Correspondence: csriram@umich.edu

Abstract

Metabolites such as acetyl-CoA and citrate play an important moonlighting role by influencing the levels of histone post-translational modifications (PTMs) and regulating gene expression. This cross talk between metabolism and epigenome impacts numerous biological processes including development and tumorigenesis. However, the extent of moonlighting activities of cellular metabolites in modulating the epigenome is unknown. We developed a data-driven screen to discover moonlighting metabolites by constructing a histone PTM-metabolite interaction network using global chromatin profiles, metabolomics, and epigenetic drug sensitivity data from over 600 cancer cell lines. Our ensemble statistical learning approach uncovered metabolites that are predictive of histone PTM levels and epigenetic drug sensitivity. We experimentally validated synergistic and antagonistic interactions between histone deacetylase and demethylase inhibitors with the metabolites kynurenic acid, pantothenate, and 1-methylnicotinamide. We apply our approach to track metabolic-epigenetic interactions during the epithelial-mesenchymal transition. Overall, our data-driven approach reveals extensive metabolic-epigenetic interactions than previously thought, with implications for reversing aberrant epigenetic alterations and enhancing epigenetic therapies.

Introduction

Metabolic reprogramming is necessary to support rapidly changing bioenergetic demands of proliferating cells such as stem cells and cancers. While the regulation of metabolism through transcriptional and signaling pathways is extensively studied, how metabolites feedback and regulate gene expression via epigenetic modifications is poorly understood[1]. Epigenetic changes like histone post-translational modifications (PTMs) are sensitive to metabolites. They can relay information about the cellular metabolic state to the genome to regulate gene expression[2, 3].

Epigenetic enzymes that “write” or “erase” PTMs on the histone tails sense levels of specific metabolites, such as S-adenosylmethionine, acetyl-CoA, and NAD+[2-4]. Glucose-derived acetyl-CoA and fatty acid-derived acetate are the substrates for histone acetyltransferases (HATs)[5, 6]. Histone deacetylases (HDACs) remove acetyl groups from acetylated lysine residues using NAD+ [7]. Histone methyltransferases (HMTs) utilize S-adenyosylmethionine (SAM) in the one-carbon metabolism and the folate cycle to install methyl groups on histone tails[8, 9] and multiple methyl groups (up to 3) can be installed to exert different expression patterns[10, 11]. Histone demethylases remove methyl groups using FAD with alpha-ketoglutarate, or another mechanism that utilizes oxygen, iron, and L-ascorbate[10, 11].

Metabolic-epigenetic interactions play a central role in controlling cellular development and physiology. For instance, the activity of the one-carbon and nicotinamide pathway impacts histone methylation levels, and acetyl-CoA levels correlate with histone acetylation in embryonic stem cells[2, 5, 12, 13]. Metabolic dysregulation can lead to altered acetylation states associated with increased cancer risk[14]. Glucose-derived acetyl-CoA correlates with histone acetylation levels and activation of oncogenes in various cancer cell models[15, 16]. Loss of function mutations in metabolic genes causes an accumulation of succinate, fumarate, and 2-hydroxyglutarate in diverse cancers. These metabolites inhibit demethylase enzymes such as the tumor suppressor TET2 and promote the epithelial-to-mesenchymal transition[2, 17, 18]. Metabolic reprogramming is essential to support the demands of a growing tumor, including sustained biomass formation, immune evasion, and metastasis[12, 19-21]. While we understand how genetic and signaling mechanisms influence metabolic dysregulation during tumorigenesis[21-23], the link between metabolism and gene expression via epigenetic regulation is poorly understood.

Epigenome-targeted therapies are emerging as a therapeutic option for several cancers, with numerous drugs currently in the preclinical and clinical pipeline[24, 25]. Vorinostat was the first HDAC inhibitor approved by the FDA to treat cutaneous T-cell lymphoma[26]. Since then, other HDAC inhibitors have been approved as anticancer agents. Additionally, several promising preclinical compounds inhibit histone methyltransferases and lysine demethylases for cancer treatment[24, 27].

Cellular metabolic status can impact efficacy of drugs, including HDAC inhibitors[25]. Notably, flux balance analysis modeling showed that the metabolic flux of acetyl-CoA in the nucleus was predictive of sensitivity to HDAC inhibitors[28]. Prior studies based on transcriptomics data have found that metabolic gene expression is predictive of anti-cancer drug sensitivity[29]. However, it is unknown how effective epigenetic therapeutics are in the context of environmental variables such as metabolite or nutrient levels. Thus, there is a need to develop tools that can predict the impact metabolism has on chromatin-modifying drugs. Further, the metabolic dependencies of epigenetic drugs can shed light on mechanistic interactions between metabolism and epigenome.

Here we apply a data-driven pipeline to discover metabolic-epigenetic interactions. We constructed an interaction network using global chromatin profiles, epigenetic drug sensitivity data, and metabolomics data from over 600 cancer cell lines in the Cancer Cell Line Encyclopedia (CCLE). Using several machine learning models, we prioritized top histone PTM-metabolite and metabolite-drug interaction pairs. Our analysis uncovered surprising metabolic dependencies of epigenetic drugs, and we validated predictions for four metabolites that had synergistic/antagonistic relationships with chromatin-modifying drugs Vorinostat and GSK-J4. We further apply our interaction network to study metabolite/PTM interaction dynamics during the epithelial-mesenchymal transition (EMT). Together, our findings provide a comprehensive resource to explore the complex relationship between cancer metabolism, epigenetics, and drug sensitivity.

Results

Systematic comparison of Histone PTM and metabolite profiles

We first evaluated the correlation profiles between intracellular metabolite levels and histone PTM levels across 623 CCLE cell lines[30, 31] (**Figure 1A**; **S. Table 1**). We hypothesized that variation in levels of metabolites will lead to a corresponding change in levels of histone PTMs they potentially regulate. Among the top 20 metabolites with the highest absolute correlation value, we found several metabolites directly or indirectly linked with histone PTM levels, including AMP, pantothenate, NAD, and 1-methylnicotinamide (1-MNAM) (**Figure 1C**). Most of the top hits were related to the one-carbon metabolism pathway that produces nucleotides, glutathione, polyamines, and SAM[32]. 1-MNAM is produced by Nicotinamide N-methyltransferase (NNMT) using SAM as the methyl donor and nicotinamide (NAM) as the substrate as a salvage mechanism[33]. While NNMT is highly expressed in various cancers and triggers epigenetic remodeling in cancer tissues, the relationship between NAM metabolism and its impact on various histone methylation sites has not been determined. Evidence suggests that 1-MNAM levels increase H3K4 methylation in mouse obesity models[34]. We found that 1-MNAM is negatively correlated with histone acetylation while positively correlated with histone di- and trimethylation levels, specifically H3K4me2, H3K9me3, H3K36me2 and H3K36me3 (**Figure 1B)**. Previous findings report that 1-MNAM upregulates histone deacetylase activity[35], supporting our observation that 1-MNAM levels correlate with lower histone acetylation levels. The positive association between histone methylation and 1-MNAM levels was expected. However, it is interesting that this relationship is statistically significant only for selected lysine sites and is not associated with all methylation marks. This analysis suggests that specific histone methylation sites may be coupled to this alternative salvage pathway mechanism, which has not been documented in the literature.

We next sought to identify histone PTMs that are highly associated with metabolism. Our analysis revealed that H3K36me1, H3K4me1, H3K23ac1, H3K9ac1, and H3K9me2 were the top 5 histone PTMs that had the highest number of statistically significant associations (p-value < 0.05, FDR < 0.25) with metabolite levels (**Figure 1D**). Previous literature supports some of these top histone PTMs. For instance, several groups have identified the role of dysregulated H3K9 and H3K4 methylation and acetylation on cancer progression and its association with glycolytic activity[16, 36]. Interestingly, our analysis suggests that H3K23ac is also highly sensitive to metabolic state but has an unidentified mechanism in the literature. Increased H3K23ac levels are associated with oncogene activation[37], potentially suggesting that H3K23ac senses metabolic processes to support oncogenesis.

The levels of several nucleotides (NTs), monophosphorylated NTs, and deoxy-NTs were found to be positively correlated with histone acetylation status across multiple lysine sites. The correlation of these NT metabolites with histone PTMs is likely due to their connection with one-carbon metabolism and cellular growth. Given that global histone acetylation is generally associated with oncogene activation[38], it is not surprising that these building blocks positively affect acetylation status. Ribose-5-P/ribulose-5-P from the pentose phosphate pathway was also positively associated with histone acetylation and is a necessary substrate for purine biosynthesis[39]. Interestingly, histone methylation has mixed associations with NT levels and is likely context-specific based on the methylation sites. To explore the impact metabolites have on gene regulation, we grouped significant correlations by PTMs with known activating/repressing functions[40, 41] (Figure 1B). We did not find any metabolites with associations specific to activation or repressive marks alone. Although the primary focus of this

study is on metabolite-epigenetic interactions, we also found several significant associations between lipids and histone PTMs (**S. Figure 1**).

We performed literature mining to confirm that we found biologically relevant metabolite/histone PTM interactions. We found 59 studies supporting several statistically significant interactions and their impact on histone PTM levels (**S. Table 2**). Many of these studies focused on metabolites that directly contribute to histone acetylation and methylation, including acetate, L-ascorbate, glucose, branched-chain amino acids, and fatty acids. Our correlation analysis also identified known epigenetic modulators AMP and NAD and several novel metabolites with unannotated functions in epigenetic regulation (**Figure 1B**). Nevertheless, several factors may confound our correlation analysis, including the effect of tissue lineage and noise in omics measurements. We next correlated metabolite levels with epigenetic drug sensitivity data; we hypothesized that this orthogonal analysis could validate metabolite-histone PTM interactions and uncover additional interactions.

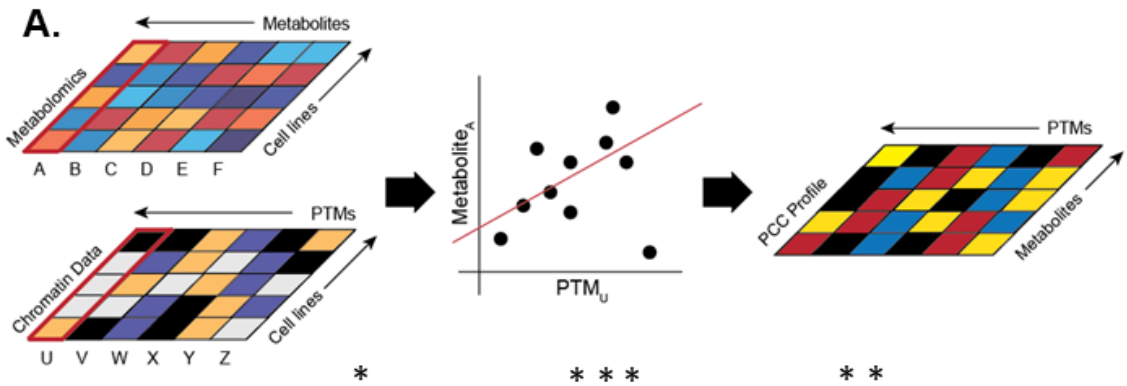
A.
Metabolites
Metabolomics
Cell lines
A B C D E F
PTMs
Chromatin Data
Cell lines
U V W X Y Z
Metabolite
PTM
PTMs
PCC Profile
Metabolites

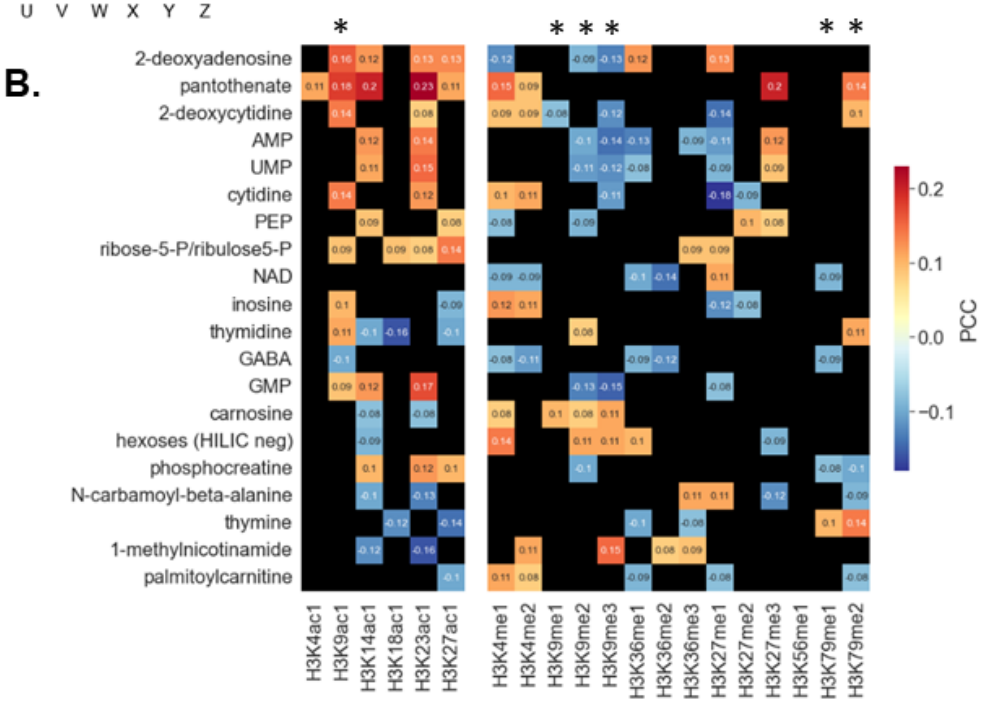
B.
2-deoxyadenosine
pantothenate
2-deoxycytidine
AMP
UMP
cytidine
PEP
ribose-5-P/ribulose5-P
NAD
inosine
thymidine
GABA
GMP
carnosine
hexoses (HILIC neg)
phosphocreatine
N-carbamoyl-beta-alanine
thymine
1-methylnicotinamide
palmitoylcarnitine
H3K4ac1
H3K9ac1
H3K14ac1
H3K18ac1
H3K23ac1
H3K27ac1
H3K4me1
H3K4me2
H3K9me1
H3K9me2
H3K9me3
H3K36me1
H3K36me2
H3K36me3
H3K27me1
H3K27me2
H3K27me3
H3K56me1
H3K79me1
H3K79me2
PCC
0.2
0.1
0.0
−0.1

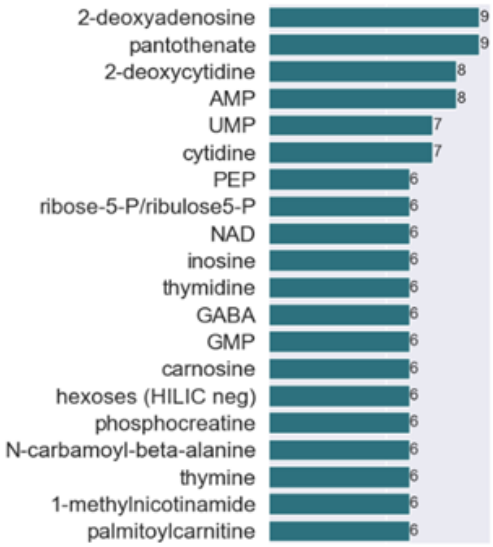
C.
2-deoxyadenosine 9
pantothenate 9
2-deoxycytidine 8
AMP 8
UMP 7
cytidine 7
PEP 6
ribose-5-P/ribulose5-P 6
NAD 6
inosine 6
thymidine 6
GABA 6
GMP 6
carnosine 6
hexoses (HILIC neg) 6
phosphocreatine 6
N-carbamoyl-beta-alanine 6
thymine 6
1-methylnicotinamide 6
palmitoylcarnitine 6

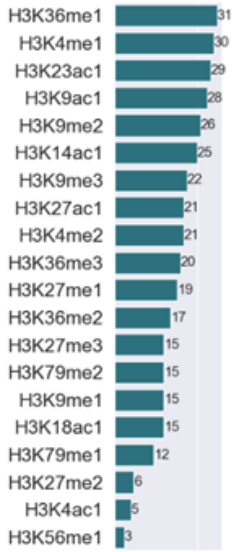
D.
H3K36me1 31
H3K4me1 30
H3K23ac1 29
H3K9ac1 28
H3K9me2 26
H3K14ac1 25
H3K9me3 22
H3K27ac1 21
H3K4me2 21
H3K36me3 20
H3K27me1 19
H3K36me2 17
H3K27me3 15
H3K79me2 15
H3K9me1 15
H3K18ac1 15
H3K79me1 12
H3K27me2 6
H3K4ac1 5
H3K56me1 3

Figure 1. Metabolite and histone PTM correlation profiles across 623 cancer cell lines
A) Schematic of generating the Pearson's correlation coefficient profile between metabolites and histone PTM data. Correlations are calculated between a PTM (example: PTM U) and metabolite (example: metabolite A) across all cell lines. This process is iterated across all metabolite and PTM combinations to generate a heatmap.
B) Histone PTM and metabolite correlation profile for the top 20 metabolites with the highest number of statistically significant interactions (p-value < 0.05; black = non-significant). The left side of the heatmap shows histone PTMs associated with gene activation, while the right-side shows histone PTMs associated with gene repression. Colors closer to red indicate a positive correlation, while blue indicates a negative correlation. Columns with asterisks indicate PTM with known gene repression actions. All other columns are PTMs with known gene activation actions.
C) Number of statistically significant metabolites (x-axis) associated with a given histone PTMs (y-axis).
D) Number of statistically significant histone PTMs (x-axis) associated with a given metabolite (y-axis). The top 20 metabolites were visualized.

Systematic comparison of metabolite levels and epigenetic drug sensitivity

We examined the relationship between metabolic states and their impact on epigenetic drug sensitivity. We analyzed data for 25 HDAC-, 5 HMT-, and 3 Histone demethylase (HDM)-inhibitors across 623 CCLE cell lines with drug sensitivity AUC values and metabolomics data[30, 42] (**Figure 2A**; **S. Table 3)**. In our analysis of the top 20 histone PTM drugs ranked by the number of significant metabolite correlations, we found 13 histone deacetylase (HDAC) and four histone methyltransferase (HMT) inhibitors (**Figure 2B**). Interestingly, we observed that the direction of the correlation (positive/negative) for each metabolite was the same between different drug classes (HDAC / HMT / HDM inhibitors). The exceptions to this observation were Repligen 136 and BRD-K80183349, suggesting that these drugs have different metabolic dependencies compared to other drugs within the same drug class.

Overall, most drugs were significantly correlated with metabolites (**Figure 2C**). Both 1-MNAM and pantothenate appeared in the top 20 metabolites with the most interactions in the metabolites/histone PTM and metabolite/drug sensitivity analyses, suggesting that there is a significant epigenetic role for these two metabolites. Additionally, glutathione and homocysteine appear in the top 20 most connected metabolites, supporting the importance of redox homeostasis and one-carbon metabolism in modulating drug sensitivity. Most drugs that have statistically significant interactions with metabolites were HDAC inhibitors (HDACi), which may be partially attributed to the distribution of drugs available in the drug response dataset (**Figure 2D**).

We next analyzed synergistic and antagonistic relationships between drug/metabolite pairs. In this analysis, a positive correlation between metabolite level and drug AUC value implies that the metabolite/drug pair is in a potentially antagonistic relationship and vice-versa for a negative correlation (a high drug AUC value indicates greater cell viability). Our analysis revealed that 1-MNAM and homocysteine were associated with antagonism, while pantothenate was associated with synergism across all drug classes (**Figure 2B**). We also observed an antagonistic association between glutathione (GSH) with various epigenetic drugs. Increased levels of GSH have been associated with drug resistance in tumor cells through several mechanisms that support the redox environment of a tumor or that directly affect the drug[43]. GSH has also been shown to inhibit S-adenosyl methionine synthetase activity[44], affecting DNA and histone methylation. Thus, the antagonistic association between GSH and histone PTM-modifying drugs could be attributed either to a direct influence on drug activity by modulating the

redox balance of the tumor microenvironment or by limiting substrate availability. Finally, when considering novel and unexpected metabolite/drug associations, we found that sorbitol had an antagonistic association across all histone PTM drug types. Sorbitol is both an osmolyte and an activator of the c-Jun N-terminal kinase (JNK) pathway, which controls various processes, including proliferation and apoptosis after DNA damage[45]. Thus, sorbitol may modulate epigenetic drug potency in multiple ways, although the exact mechanism is not clear.

To complement our metabolite-histone-PTM and drug sensitivity correlation analysis and ensure that we can capture biologically relevant associations with our dataset, we evaluated the correlation between histone PTM levels and histone PTM drug sensitivity data. (**S. Figure 2**). A negative correlation of PTM levels with drug sensitivity implies increased PTM levels are associated with decreased cell viability. We expected a negative correlation between histone acetylation levels and HDAC inhibitor AUCs since HDAC inhibitors promote cell death via hyperacetylation. We found that our analysis could support our expectation and all statistically significant correlations were negative (**S. Figure 2D;** p-value < 0.05). We found that HDAC inhibitors - Vorinostat, Tacedinaline, and Apicidin, were the top three drugs with the highest association with histone PTM levels (**S. Figure 2A**). While most histone PTMs were correlated with the drugs in the dataset, H3K27me1, H3K56me1, and H3K4ac1 did not have any statistically significant correlations (**S. Figure 2B**). Interestingly, the association between histone methylation levels and methylation-related drug sensitivity data is unclear. We found several statistically significant positive and negative correlations between histone methylation levels and their respective HMT/HDM drug classes (**S. Figure 2C**), which was unexpected. HMT and HDM inhibitors had fewer statistically significant associations overall (**S. Figure 2A**). Finally, we examined which histone PTMs had the highest number of statistically significant associations with drug sensitivity (**Supplementary Figure 2A & B; S. Table 4**). Among the acetylation PTMs, the most predictive lysine sites were H3K23, H3K14, H3K18, and H3K27.

Our correlation profiles revealed several important metabolite-PTM, metabolite-drug, and PTM-drug interactions across 623 cancer cell lines of different tissue lineages and genetic profiles. The findings from our correlation analysis were used to inform our drug profiling experiments, described in a later section.

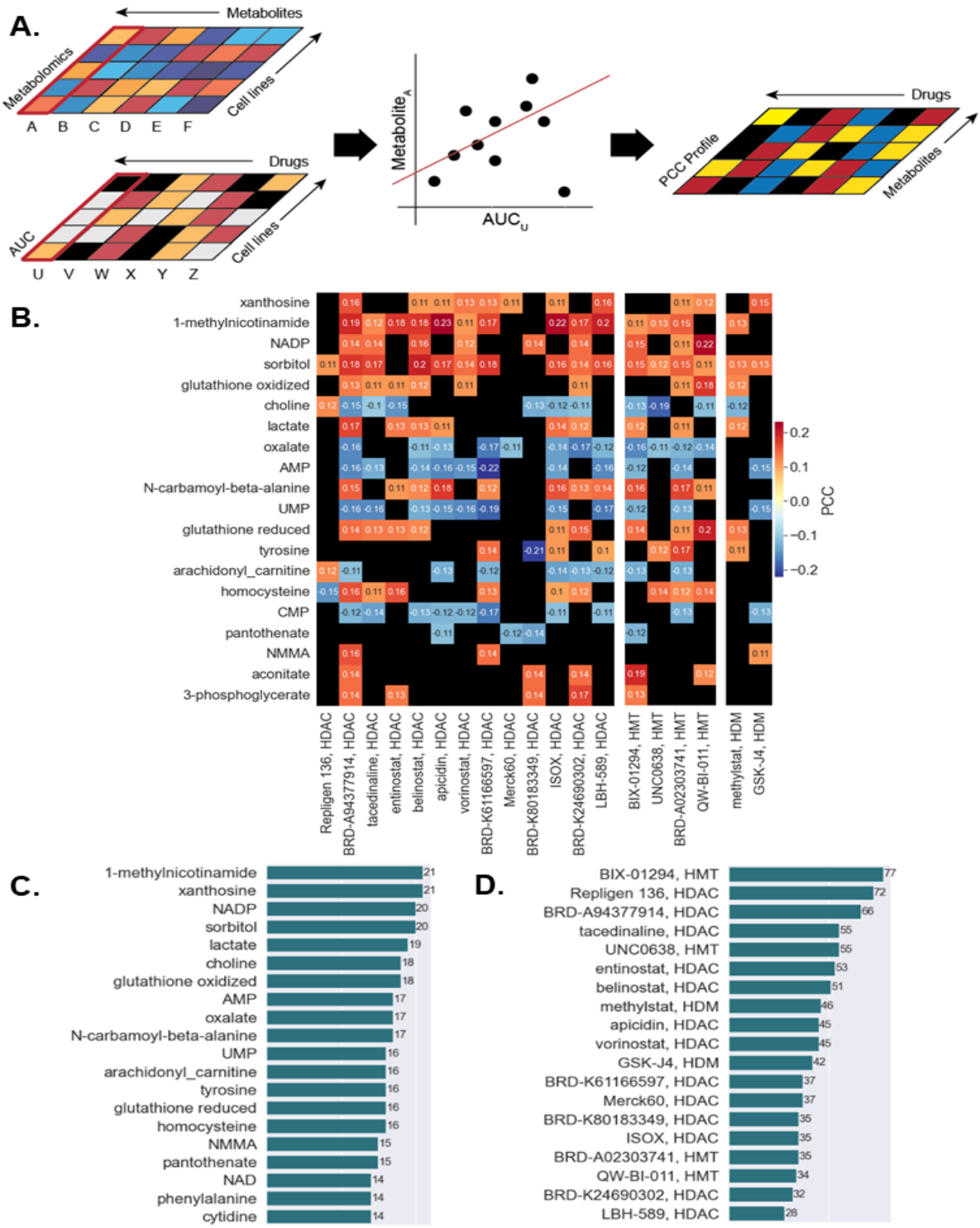

Figure 2. Metabolite and drug sensitivity correlation profiles across 623 cancer cell lines
A) Schematic of generating the Pearson's correlation coefficient profile between metabolites and histone modifying drug AUC data. Correlations are calculated between a drug (example: drug U) and metabolite (example: metabolite A) across 623 cell lines. This process is iterated across all metabolite and drug combinations to generate a heatmap.

B) Drug and metabolite correlation profile for the top 20 metabolites with the highest number of statistically significant interactions (p-value < 0.05, FDR < 0.25; black = non-significant). The x-axis is divided into three classes of inhibitors: HDAC, HMT, and HDM. Colors closer to red indicate a positive correlation, while blue indicates a negative correlation.
C) Number of statistically significant metabolites (x-axis) associated with a given drug (y-axis).
D) Number of statistically significant histone-modifying drugs (x-axis) associated with a given metabolite (y-axis). The top 20 metabolites were visualized.

Inferring PTM, metabolite, and drug sensitivity interactions using statistical learning

While correlation analysis has identified important metabolic-epigenetic relationships, correlation does not identify non-linear and combinatorial associations between many features. To address these issues, we leveraged three statistical learning methods that are simple to interpret to map the associations between metabolite levels, drug sensitivity, and histone PTM levels (**Figure 3**). We used the k-Top Scoring Pair algorithm (k-TSP), which measures ratios of metabolites. We used this approach since many cellular processes are sensitive to relative levels of metabolites (e.g., NADH/NAD) rather than absolute levels. In addition, LASSO and stepwise regression were used to get the minimal number of metabolites in combination that best predict either a given histone PTM or drug AUC value (**Figure 3A**).

We first analyzed individual machine-learning model findings as each model uncovered a distinct set of interactions. The LASSO method performs feature selection to prioritize top interactions (**Methods**). We used the LASSO coefficients to construct a bidirectional directed network to quantify the interactions between histone PTMs and metabolite levels (**S. Figure 3; S. Table 5**). We found that H3K14ac1, H3K23ac1, and H3K4me1 were the histone PTMs with the most significant associations between multiple metabolites in the interaction network.

Additionally, we found several metabolites that are known to support both acetylation and methylation processes. Methionine, threonine, and 1-MNAM from one-carbon metabolism were associated with the H3K4me1, while phosphorylated sugars from glycolysis (F1P/F6P/G1P/G6P) and branched-chain amino acids were linked with H3K14ac1 (**S. Figure 3**). These are consistent with prior studies linking these metabolites with histone PTMs[46, 47]. Notably, these metabolites were not identified in our correlation analysis. This is likely due to the LASSO model identifying multivariable and combinatorial relationships in the metabolomics dataset. These suggest that the histone PTMs are potentially sensitive to relative levels of these metabolites in relationship with other metabolites.

Other notable metabolite/PTM interactions include the positive associations between pantothenate and H3K4me1, the shared interaction between L-sorbitol and 1-MNAM with H3K4me1 and H3K23ac1, and the negative association between kynurenic acid and H3K23ac1. When we examined the relationship between 1-MNAM and these PTMs, we found that 1-MNAM had a negative association with histone acetylation while having strong positive associations with H3K4me1 (**S. Table 5**). A positive association between 1-MNAM and H3K4me1 was expected, as 1-MNAM is a methyl acceptor and can potentially affect methyl substrate levels. However, 1-MNAM and its specific association with H3K4me1 provides insights into the context specificity 1-MNAM may have on epigenetic regulation.

While our analysis revealed that metabolites 1-MNAM and kynurenic acid were highly associated with different histone methylation and acetylation marks, Li *et al.*,2019 found that

strong lineage effects are associated with these metabolites[30]. To confirm whether this is a real biological signal, we experimentally assessed the impact 1-MNAM and kynurenic acid had on cancer drug sensitivity in a later section.

The LASSO interactions between drug AUC values and metabolite levels revealed that several metabolites had negative coefficients with both the histone demethylase inhibitor GSK-J4 and Vorinostat AUC values, suggesting that higher levels of metabolites within the network contribute to lower drug AUC or increased drug sensitivity (**S. Figure 4; S. Table 6**). One interaction we were interested in was the synergistic link between GSK-J4 and kynurenic acid. Kynurenic acid is known for its anti-inflammatory and immunosuppressive functions that support cancer progression[48]. Kynurenic acid has been shown to impact histone methylation patterns in microglial cells to support anti-inflammatory phenotypes[49]. Despite this observation in neuropathology, the association of kynurenic acid modulating cancer epigenetics has not been investigated.

While the LASSO interaction network is intuitive, the large number of associations is still a barrier to interpretation. Therefore, we trained simpler stepwise-regression models that only considered a single metabolite, two metabolite, or three metabolite models that best-predicted histone levels (**S. Figure 5; S. Table 7**). Across all our models, we found that pantothenate, leucine, and 1-MNAM were top predictors of histone PTM levels and drug sensitivity.

Since correlations, LASSO, and stepwise regression models assume a univariate linear contribution to each output, we used the k-TSP model to assess bi-variate interactions. This modeling approach evaluates the interactions two metabolites have on a given histone PTM with a given probability. We also assessed predictions from other machine learning models and found k-TSP to provide both relatively high accuracy and interpretability (**S. Methods**). k-TSP identified 1-MNAM with lactose and kynurenic acid contributed strongly to histone PTM predictions, specifically H3K23ac1 and H3K9me3. We also evaluated which PTM pairs are predictive of metabolite levels, focusing on 1-MNAM. We found that H3K23ac1/H3K9me3 and H3K14ac/H3K79me2 were highly predictive of 1-MNAM (**S. Figure 6A-C**). Finally, we focused on H3K9me3, a histone PTM involved in several biological processes related to cancer. Our analysis revealed that 1-MNAM with palmitoylcarnitine and 5-adenosylhomocysteine with aconitate predict H3K9me3 levels (**S. Figure 6D-E**).

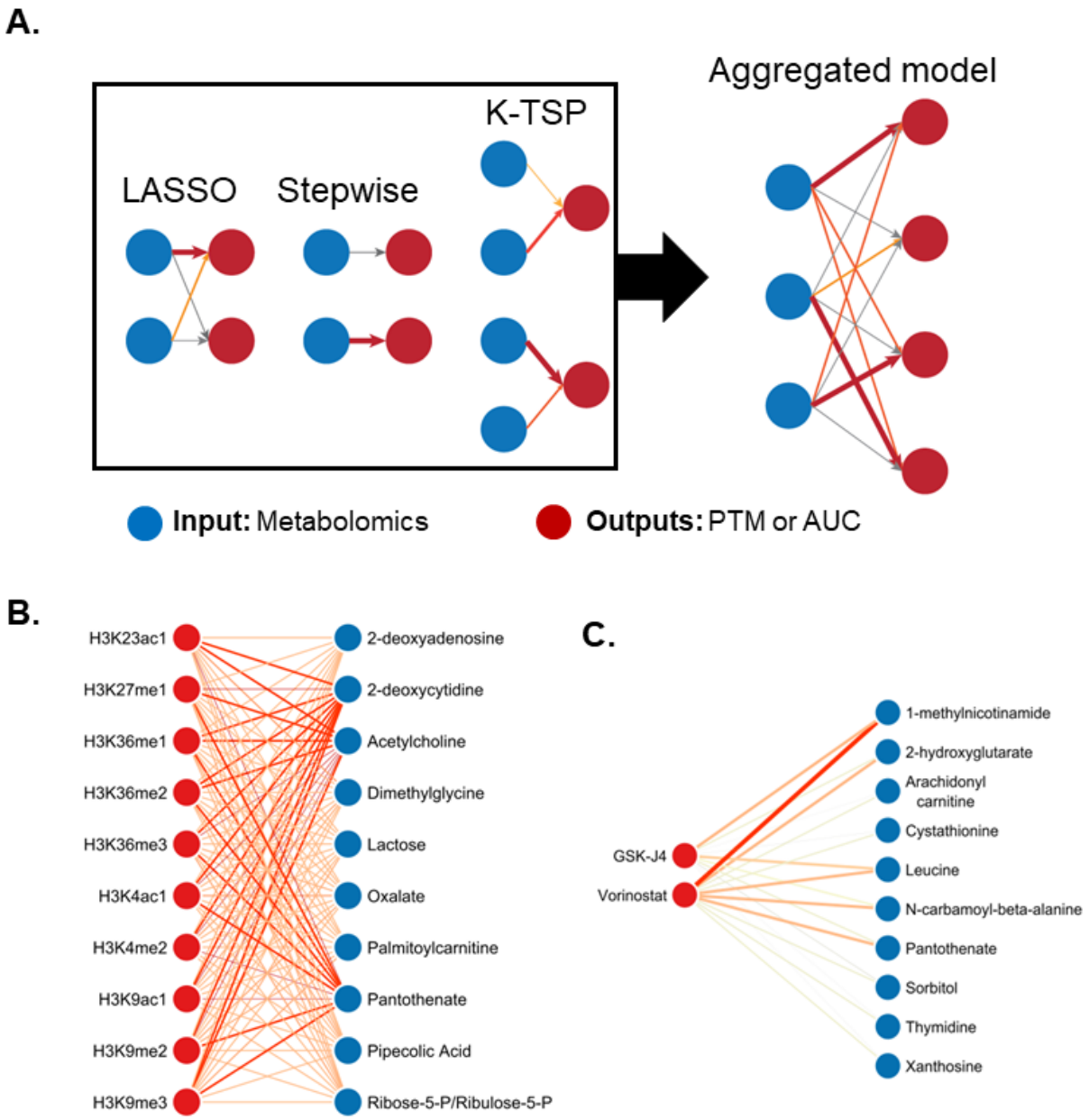

Figure 3. Inferring metabolite-PTM-drug sensitivity interactions using machine learning
A) Model schematic. Three machine learning models were trained on metabolomics data (input: metabolomics, blue nodes) to predict histone PTM levels and drug AUC values (output; red nodes). The absolute value of the coefficients for the LASSO and stepwise regression models and the Pearson correlation coefficient of the K-TSP true/predicted outputs were combined over the union using a product operation. The meta-model coefficients were weighted by the number of experiments that intersected across the models. The edge color (gray: weak to red: strong) indicates the strength of the relationship between the two nodes. Top interactions consistent across multiple methods are visualized in panels B and C. See **S. Tables 8 and 9** for a complete list of all interactions.
B) Top meta-model relationships between metabolite levels and histone PTM predictions. Red nodes indicate PTMs. Blue nodes indicate metabolites.

C) Top meta-model relationships between metabolite levels and GSK-J4 and Vorinostat drug AUC levels. Red nodes indicate histone-modifying drugs. Blue nodes indicate metabolites.

We combined the coefficients from all these models into a single meta-model to identify the most robust interactions under different statistical assumptions. The top 20 metabolites containing the highest consolidated coefficients were selected for discussion.

2-deoxycytidine, acetylcholine, and pantothenate had the highest associations with several histone PTM levels in the meta metabolite-PTM model (**Figure 3B; S. Table 8**). From our correlation analysis, pantothenate was highly predictive of histone acetylation markers (**Figure 1A**), which is expected due to its role in coenzyme A biosynthesis[50]. Pantothenate was highly predictive of H3K4ac and, to some extent, H3K9ac and H3K23ac across multiple models. Surprisingly, a strong relationship emerged between pantothenate and several histone methylation marks suggesting that coenzyme A may have a cross-functional regulatory role with histone methylation. However, there was no reported experimental evidence supporting this finding.

We specifically looked at two histone-modifying drugs that were highly correlated with metabolite levels. These two drugs were Vorinostat, an HDAC inhibitor that targets most HDACs, and GSK-J4, an H3K27me2/3 demethylase inhibitor[51, 52]. Both drugs have been FDA-approved for cancer treatment: Vorinostat is a treatment for cutaneous T-cell lymphoma and is in clinical trials for several cancers, while GSK-J4 is a treatment for glioblastoma[53]. The strongest interaction between our three models was between Vorinostat and 1-MNAM (**Figure 3C; S. Table 9**). A previous study has shown that 1-MNAM stabilizes the deacetylase enzyme SIRT1[54] and may also impact the activity of other deacetylases. Our machine learning approach supports this hypothesis by predicting its association with Vorinostat. GSK-J4 was also associated with 1-MNAM and leucine across multiple machine learning models (**Figure 3C; S. Table 9**). Given the role of 1-MNAM as a methyl acceptor and its impact on SIRT1, its potential to regulate acetylation and methylation status is intriguing. It suggests crosstalk between acetylation and methylation. We summarize our findings for metabolite/PTM interactions (**S. Table 10**) and metabolite/drug interactions (**S. Table 11**) that are common across multiple machine learning and statistical models.

Tracing metabolite-epigenetic changes during the epithelial-to-mesenchymal transition (EMT)

As a proof of concept of how the inferred network can be used to understand metabolic-epigenetic interactions in various contexts, we applied our model to the EMT system. EMT is a reversible developmental process that facilitates the transition from an epithelial cell to a mesenchymal cell with stem-cell-like properties[55]. Extensive metabolic and epigenetic changes occur during EMT, which may contribute to tumor heterogeneity, drug resistance, and metastasis[56]. Understanding how multiple biological processes promote EMT in cancer is essential to developing therapeutic strategies.

We applied our meta-network to track changes observed in metabolomics and histone proteomics data in cancer cell lines undergoing EMT[57, 58] (**Figure 4; S. Figure 7**). Overlaying the histone PTM data onto the metabolite/PTM network showed that most changes occurred during the first 24-hour period. H3K4me2 showed the largest decrease, and H3K9ac showed the largest increase in levels relative to the 0th hour (**S. Figure 7**). We next applied our trained

LASSO models to quantitatively predict changes in PTM levels over time using time-course metabolomics and histone PTM proteomics data. The data was centered on the same scale as the CCLE training set (**Methods**). We evaluated the quality of our predictions by comparing the mean-squared error between the predicted values against the true PTM levels (**Figure 4B**). Overall, most histone PTMs were predicted to have a low MSE, showing that our LASSO model was generalizable across datasets. The two histone PTMs our LASSO model could not predict well were H3K4me2 and H3K27me1, suggesting heterogeneity and context-specificity of their expression. To understand the metabolites driving these predictions, we next visualized the metabolomics data onto the LASSO metabolism-PTM network (**Figure 4C**). The most pronounced changes in epigenome-predictive metabolite levels were increased glycolytic metabolites F1P/F6P/G1P/G6P and dimethylglycine (DMG). These observations corroborate previous studies, where increased glycolysis and one-carbon metabolism were associated with EMT[59-61]. While increased glycolysis may drive increased histone acetylation, DMG and one-carbon metabolites are predicted to be negatively correlated with acetylation, which may explain the overall lack of a significant increase in acetylation (**Figure 4C**).

Analysis of the metabolite-drug network for A549 cells undergoing EMT revealed that 1-MNAM increased from 24-72 hours based on the metabolomics data, which is strongly associated with Vorinostat drug sensitivity (**Figure 4A**) while having a comparatively lower impact on GSK-J4 drug sensitivity. However, in HCC827 cells, 1-MNAM levels reduce after 24hrs during EMT, suggesting reduced Vorinostat sensitivity[57]. Vorinostat displays a dual response of inducing and inhibiting EMT in a context-dependent manner[62, 63]. Our model captures the context-specific heterogeneity in Vorinostat response based on metabolic state.

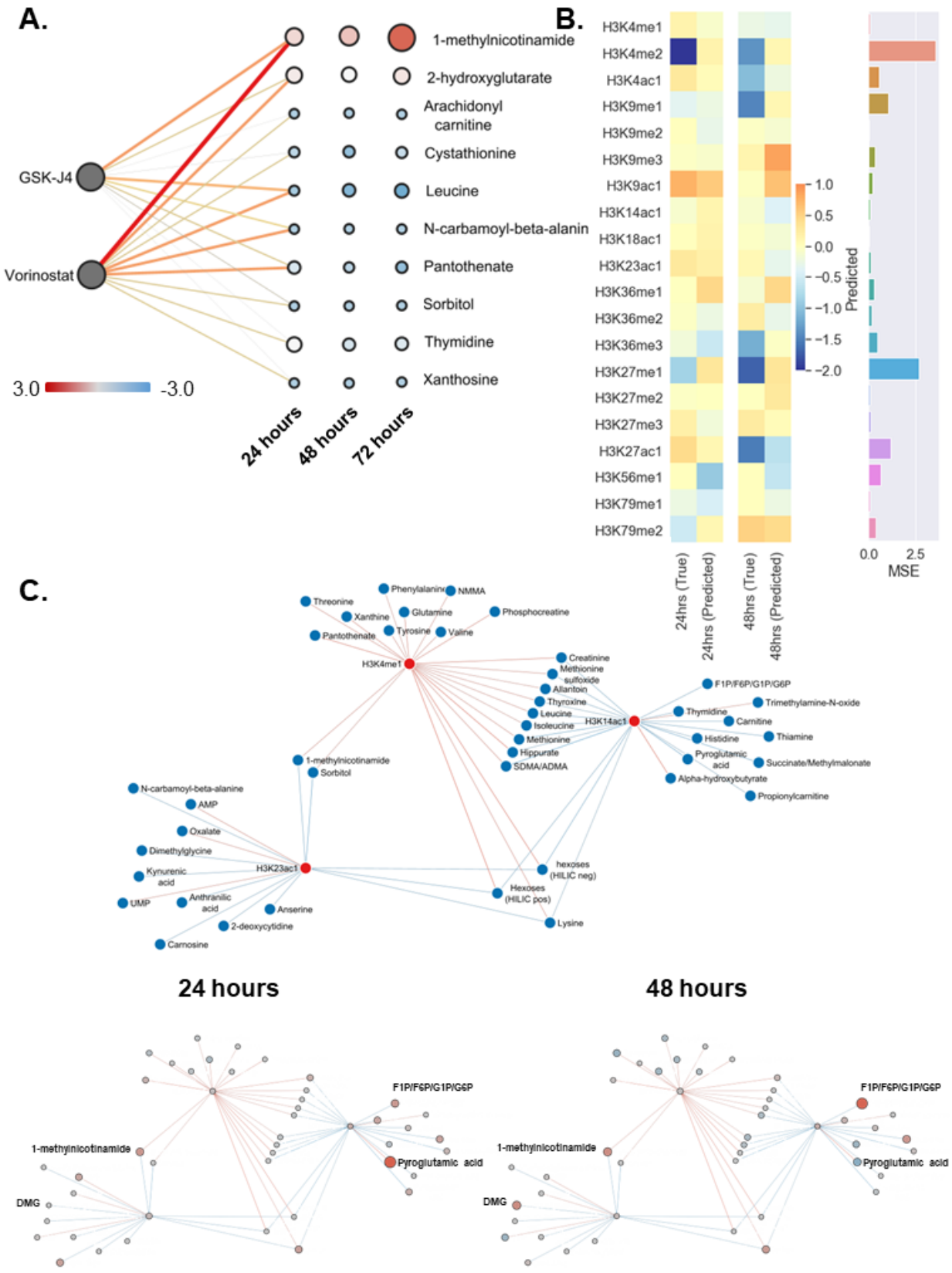
A.
GSK-J4
Vorinostat
1-methylnicotinamide
2-hydroxyglutarate
Arachidonyl carnitine
Cystathionine
Leucine
N-carbamoyl-beta-alanin
Pantothenate
Sorbitol
Thymidine
Xanthosine
3.0
-3.0
24 hours
48 hours
72 hours
B.
H3K4me1
H3K4me2
H3K4ac1
H3K9me1
H3K9me2
H3K9me3
H3K9ac1
H3K14ac1
H3K18ac1
H3K23ac1
H3K36me1
H3K36me2
H3K36me3
H3K27me1
H3K27me2
H3K27me3
H3K27ac1
H3K56me1
H3K79me1
H3K79me2
1.0
0.5
0.0
−0.5
−1.0
−1.5
−2.0
Predicted
0.0
2.5
MSE
24hrs (True)
24hrs (Predicted)
48hrs (True)
48hrs (Predicted)
C.
Threonine
Phenylalanine
NMMA
Xanthine
Glutamine
Phosphocreatine
Pantothenate
Tyrosine
Valine
H3K4me1
Creatinine
Methionine sulfoxide
Allantoin
Thyroxine
Leucine
Isoleucine
Methionine
Hippurate
SDMA/ADMA
H3K14ac1
F1P/F6P/G1P/G6P
Trimethylamine-N-oxide
Thymidine
Carnitine
Histidine
Thiamine
Pyroglutamic acid
Succinate/Methylmalonate
Alpha-hydroxybutyrate
Propionylcarnitine
1-methylnicotinamide
Sorbitol
N-carbamoyl-beta-alanine
AMP
Oxalate
Dimethylglycine
Kynurenic acid
H3K23ac1
UMP
Anthranilic acid
Anserine
2-deoxycytidine
Carnosine
hexoses (HILIC neg)
Hexoses (HILIC pos)
Lysine
24 hours
48 hours
F1P/F6P/G1P/G6P
1-methylnicotinamide
Pyroglutamic acid
DMG
F1P/F6P/G1P/G6P
1-methylnicotinamide
Pyroglutamic acid
DMG

Figure 4. Assessing the metabolic impact on drug sensitivity during the Epithelial-to-Mesenchymal (EMT) transition.
A. EMT time-course metabolomics[57] was measured from 0-72 hours, and the relative values are overlaid onto the meta-model network predictions using metabolomics to predict Vorinostat and GSK-J4 drug sensitivity in **Figure 3**. Log2 fold change (LFC) of the metabolomics (24 hours / 0 hour) is shown, where red is a positive LFC, gray is an LFC close to 0, and blue is a negative LFC. The size of the metabolite node is the absolute value of the LFC. Metabolites that did not intersect between the CCLE and the metabolomics data include arachidonyl carnitine, xanthosine, sorbitol, and N-carbamoyl-beta-alanine.
B. LASSO predictions on Nakasuka et al., 2021 metabolomics data to predict[58] histone levels during EMT. Barplot shows mean-squared error (MSE) for both 24 and 48hrs. Heatmaps show predicted values and LFC for histone PTM data for 24 and 48 hrs.
C. LASSO network showing the relationship between metabolomics and histone PTM LFC.

Validating synergistic and antagonistic metabolite and epigenetic drug interactions

Nutrient status significantly impacts drug sensitivity in cancer. For instance, dietary methionine restriction increased sensitivity to radiation and chemotherapy-resistant mouse models[64]. While this emerging area of study has promise in improving therapeutic outcomes, the interactions between nutrient supplementation and epigenetic drug sensitivity have not been systematically characterized.

Our model results identified 1-MNAM, pantothenate, kynurenic acid, glutathione, and sorbitol as important histone PTMs and drug sensitivity predictors. To validate our predictions, we performed a metabolite/drug combination screen to assess how these metabolite/drug interactions impact cancer cell proliferation (**Figure 5A**).

We ran our metabolite/epigenetic drug screen using A549 as the cancer cell line model with epigenetic drugs Vorinostat and GSK-J4. We ran the synergy/antagonism screen with an eight-point drug concentration profile with three concentrations of metabolite supplementation (**Methods**). When we evaluated the dose-response curves using DMSO as the control, we found a dose-dependent response across all metabolite and drug-treated samples (**S. Figure 8**).

Notably, GSK-J4 demonstrated significant synergy across all metabolites except sorbitol, which exhibited an antagonistic effect at high concentrations and synergy at a lower dose (**Figure 5B**). When we evaluated Vorinostat/metabolite combinations, we found a neutral effect with 1-MNAM, a stronger synergistic effect with pantothenate, and mild antagonism with both sorbitol and glutathione. The synergistic effect pantothenate has on HDAC inhibitor, and histone demethylase inhibitor suggests that it has multiple roles in epigenetic regulation and cellular survival that have not been reported in the literature. The antagonism of glutathione supplementation with Vorinostat aligns well with a recent study that showed that ablation of the cystine-glutamate antiporter (xCT) and reduction in the intracellular glutathione level increased sensitivity to Vorinostat[65]. Ablation of xCT limits the availability of cystine, a rate-limiting precursor of glutathione, thus reducing intracellular glutathione and allowing ROS accumulation that sensitizes the cells to Vorinostat.

Further, we found that high sorbitol levels antagonized the efficacy of both drugs. While our experimental results agree with our model predictions, we must acknowledge that our analyses have confounding factors. The metabolomics data we used in our correlation analysis measured internal levels of sorbitol, while our assay supplements sorbitol to the medium. External sorbitol application in cell culture results in mild osmotic stress[66], which may affect cell proliferation.

To tease out dose-specific interactions, we assessed significant pairwise metabolite and drug interactions and their impact on cell viability (**S**. **Figure 9**). To filter out noise from the dataset, we applied a p-value threshold to identify interactions with a discernible difference in the average cell count between treatment and control (two-sample T-test p-value threshold < 0.05). Our p-value filter found significant antagonistic interactions between 1-MNAM and glutathione with Vorinostat at lower metabolite doses (**S. Figure 9B**), which was predicted from our correlation analysis (**Figure 2B, 3C**). Most metabolite combinations showed a statistically significant synergistic effect with GSK-J4 (**S. Figure 9A**). On average, interactions were significant at the higher drug doses and across all three metabolite concentrations for all metabolites. However, pantothenate and GSK-J4 show a dose-dependent relationship on cell viability with the highest levels of pantothenate, suggesting a strong synergistic relationship between pantothenate and GSK-J4.

While our correlation analysis did not reveal statistically significant metabolite/drug correlations for 1-MNAM, glutathione, kynurenic acid, and pantothenate with GSK-J4, our statistical learning models allowed us to identify these significant interactions for the first time. In addition to sorbitol/GSK-J4, sorbitol/Vorinostat, and glutathione/Vorinostat, we predicted kynurenic acid having a synergistic interaction due to its negative LASSO coefficient with GSK-J4 (**S. Figure 4**). Our analyses did not show any significant association between kynurenic acid and Vorinostat, which was also captured in our assay results. Interestingly, our correlation analysis suggested that 1-MNAM was antagonistic to Vorinostat. However, the relationship is hard to determine as the combination shows antagonism at lower drug doses and synergy at higher doses (**Figure 5B**). Our machine learning analysis captured this ambiguity, which did not predict synergy/antagonism between 1-MNAM and Vorinostat.

While analysis of drug AUC data alone captured some synergistic/antagonistic interactions, augmenting with histone PTM levels helped us comprehensively identify additional epigenetic modulators. One example was pantothenate, which showed strong correlations and associations with histone PTM levels but not with the drug AUC data. When tested experimentally, we found strong synergy with both GSK-J4 and Vorinostat. In addition, choosing data mining methods with different statistical assumptions like LASSO, correlation coefficients, and kTSP allowed us to comprehensively capture interactions that each technique would have missed individually.

Potential mechanisms linking metabolites and GSK-J4

To further verify our assay outcomes, we analyzed our model predictions and literature evidence that could explain the synergistic drug-metabolite interactions. GSK-J4 affects H3K27 methylation by inhibiting the demethylase KDM6A and KDM6B[52]. Pantothenate is predicted to increase H3K27me3 based on both correlation and regression models. Thus, their synergistic

growth inhibition may be mediated through synergistic hypermethylation at H3K27me3. Metabolites that directly affect acetylation such as pantothenate may also indirectly increase H3K27 trimethylation through acetylation and subsequent stabilization of the H3K27me3 methylase EZH2[67]. Acetylation of EZH2 requires acetyl-CoA thus potentially linking these two modifications. Consistent with this, the surprisingly positive correlation between pantothenate and H3K27me3 is lost in EZH2 loss of function mutant CCLE cell lines (R = -0.44, N = 16 cell lines), and is maintained in cell lines with gain of function mutants (R = 0.51, N = 9 cell lines).

The interaction between kynurenine and GSK-J4 is especially surprising as there are no reported interactions between kynurenine with H3K27me3 or GSK-J4. GSK-J4 is being explored for treatment of gliomas[68]. Further kynurenine can cross the blood brain barrier and has been associated with glioma pathophysiology[69]. Hence its interaction with GSKJ4 might be clinically relevant for treatment of brain cancers. Analysis of Chip-seq data from GSK-J4 treated diffuse intrinsic pontine glioma (DIPG) cells revealed that IDO1 is the most differentially methylated gene at H3K27[68] (log fold change = -1.3, p-value = 0.015 for treatment vs control). The corresponding IDO1 transcript is also significantly differentially expressed after GSK-J4 treatment (log fold change = 0.41, p-value = 0.054 for treatment vs control). Kynurenine is derived from tryptophan metabolism and IDO1 represents the rate limiting step of kynurenine formation[70]. Analysis of metabolomics data from glioma cell lines that harbor a H3K27 mutation, which prevents methylation, also revealed that kynurenine and tryptophan are significantly downregulated due to the mutation compared to the wild type (log fold change = -0.22 and -0.24, p-value = 0.04 and 0.008 for kynurenine and tryptophan respectively, treatment vs control)[71]. These results suggest that kynurenine is regulated by H3K27 trimethylation. Perturbations through GSK-J4 or mutations in H3K27 impact kynurenine metabolism. Kynurenine in turn may affect H3K27 methylation directly or indirectly via H3K4 methylation as predicted through our correlation analysis.

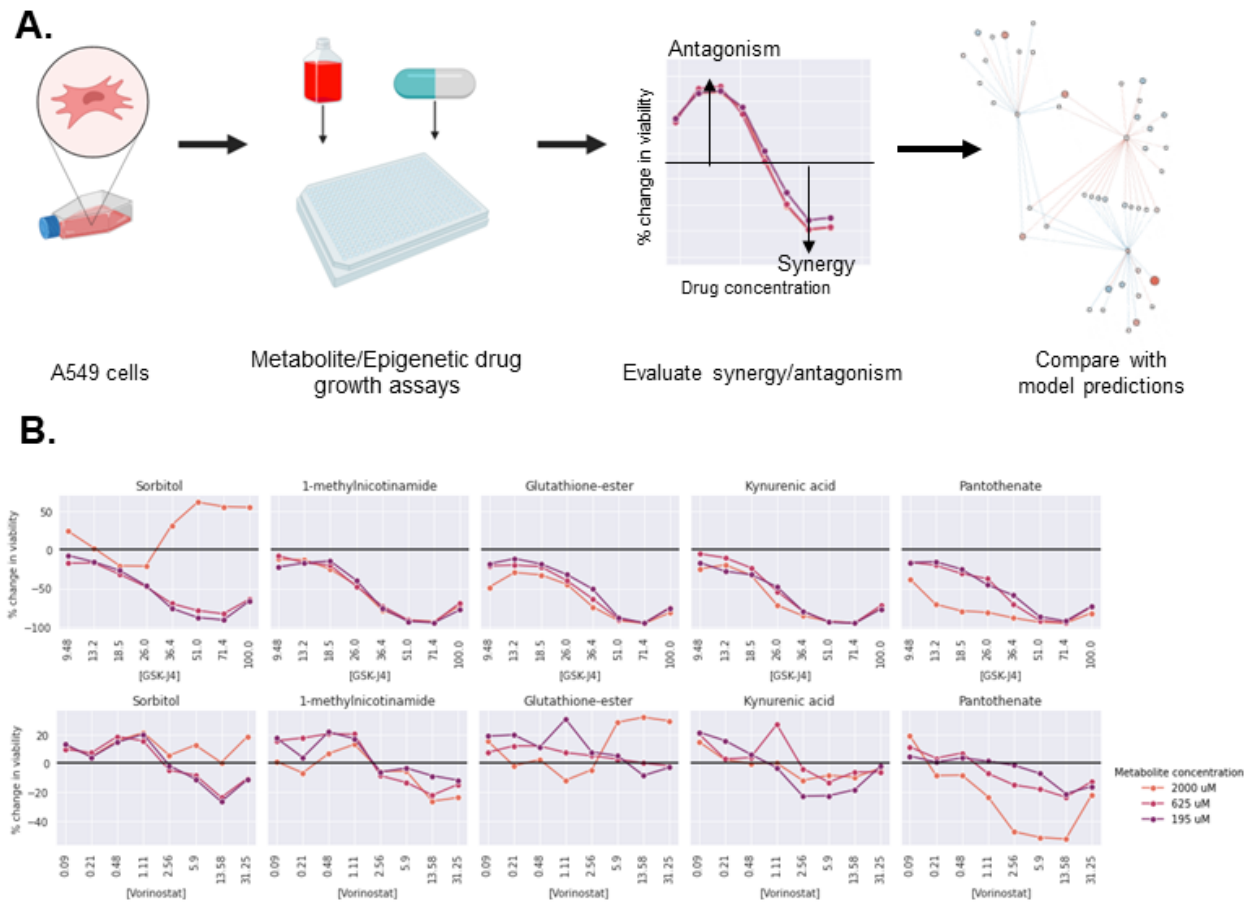

Figure 5. Metabolite/drug dose-response curves to validate model predictions for Vorinostat and GSK-J4 in A549 cells
A. Schematic of the experimental procedure.
B. Percent viability curves (treatment/control) for five metabolites + epigenetic drugs Vorinostat and GSK-J4. Control was the drug-only condition. The black line indicates no difference between treatment and control. Data points were averaged across replicates (N=2 treatment replicates; N=12 control replicates). Negative percent values below the black bar indicate synergy, while positive percent values indicate antagonism.

Discussion

Here we use a novel multi-omic statistical learning framework to study how cellular metabolism impacts histone PTMs and epigenetic drug sensitivity. Our study leverages LASSO, stepwise, and k-TSP algorithms to capture the non-linear and combinatorial interactions between metabolites and histone PTMs. Together, our model suggests that histone PTM levels can be influenced by several metabolites that are not known to be direct substrates for histone writers and erasers. Through a literature search, we identified 27 metabolites across 59 independent studies that had prior known effects on histone acetylation and methylation levels (**S. Table 2**). Our model predicted novel metabolite-PTM and metabolite-drug interactions, such as kynurenic acid with H3K23ac and GSK-J4. Assessment of our model suggests that PTMs

are potentially sensitive to the relative levels of metabolites to other metabolites. This diverse range of metabolic sensitivities for various histone PTMs may be related to the number of enzymes regulating each PTM, their kinetic properties, and their interactions with metabolic enzymes and other epigenetic factors.

Our model identified metabolites participating in one-carbon metabolism, including threonine, methionine, cystathionine, and dimethylglycine, to interact with histone PTMs and epigenetic drugs[72, 73]. Our LASSO model found that these metabolites also interact with H3K14ac and H3K23ac, which has not been reported previously. Additionally, our meta-model found that 2-hydroxyglutarate (2HG), an oncometabolite produced from IDH1/2mt[74, 75], was associated with Vorinostat sensitivity. A recent study reports that IDH1-mutant cancers are sensitive to Vorinostat by suppressing homology-directed DNA repair in cells producing 2HG[76]. Thus, these independent studies support our model's predictions.

Kynurenic acid was predicted to have a synergistic relationship with GSK-J4 (**S. Figure 4**). Interestingly, the correlation model also predicted a negative relationship between kynurenic acid and H3K27me3 levels. Analysis of chip-seq datasets after GSK-J4 treatment revealed that kynurenic acid metabolism is regulated by H3K27 methylation. These results suggest a potential feedback regulation between metabolites and the corresponding PTMs they influence. The diverse impact of kynurenic acid on the epigenome mirrors its myriad impact on biological processes including neurological, immunomodulatory and anti-cancer effects[77]. The synergistic interaction with GSK-J4 may have clinical implications for treating gliomas that frequently exhibit mutations in H3K27 and dysregulation of kynurenic acid pathway[69, 78, 79].

Pantothenate, a precursor of CoA biosynthesis[50], showed a strong correlation with PTM levels and a synergistic effect in combination with GSK-J4 and Vorinostat. Manipulating CoA levels can influence the degree of protein acetylation, which supports our experimental results, with pantothenate having a synergistic effect with Vorinostat. However, its synergy with GSK-J4 needs further experimental evaluation and may be mediated via EZH2, a H3K27 methyltransferase.

Our model also found that 1-MNAM interacts with various histone PTMs, which may explain its diverse biological effects. 1-MNAM enhances the mesenchymal phenotype in cancer cells[80, 81] by increasing the deacetylase enzyme SIRT1[54]. A recent study found that 1-MNAM is also a critical immunomodulator within the tumor microenvironment[82] and infectious diseases such as COVID-19[83].

A limitation of our study is that we do not probe the exact mechanism underpinning these inferred metabolite/PTM/drug interactions. However, we do find that these interactions are robust across hundreds of cell lines, and their mechanistic connections can be reasonably explained. Our approach prioritized the strongest metabolite/PTM and metabolite/epigenetic drug interactions, which were further scrutinized using the consolidated result of multiple machine learning models with different statistical assumptions and model complexity. Finally, the top predictions that passed these analytical thresholds showed synergistic/antagonistic effects in our drug/metabolite experiments. Further, while histone acetylation and methylation are some of the most well-understood epigenetic markers, the epigenome consists of hundreds of PTMs and non-coding RNAs[84, 85]. Although not considered here, our study provides a framework to understand the metabolic dependencies of these less-studied modifications.

Overall, our model identified critical metabolite-PTM and metabolite-drug interactions that were previously unidentified. These results provide new insights into metabolic control of the epigenome, and call attention to the impact of nutrient conditions on epigenomic assays,

which is usually not considered. Our study can also shed light on the epigenetic effects of metabolites and other nutrients within the tumor microenvironment (TME). TME is a critical regulator of tumor progression and metastasis and plays a role in acquiring drug resistance to various chemo- and radiation therapies[86-88].

The methodology outlined in this study can enable precision medicine applications. For instance, metabolomics can be used to generate hypotheses on epigenetic alterations and help prioritize epigenetic therapies. Furthermore, metabolite modulators of epigenetic therapies can be used to design specialized diets that enhance drug efficacy. HDAC inhibitors and epigenetic therapies are being explored for numerous cancers, immune- and neurological-diseases, and our results are potentially relevant to these diseases.

Methods

CCLE Data Preprocessing

Metabolomics[30] and H3 global chromatin profiling[31] data were obtained from the Cancer Cell Line Encyclopedia (CCLE), while drug sensitivity data[42] was obtained from the Cancer Therapeutics Response Portal (CTRP). We used Broad Institute IDs to map across the various datasets, resulting in 623 cancer cell lines intersecting across all datasets. The data was transformed into a Z-score prior to downstream analyses for the metabolomics and global chromatin profile data. The CTRP data was left as-is for the correlation analysis or scaled using a minimum-maximum scaler function across each drug for machine learning to reduce the data dimensionality by its range. K-nearest neighbor imputation was performed to fill in missing values using the scikit-learn library and default arguments.

We chose to reduce the dimensionality of the datasets by focusing on the interpretability of our results. Histone PTMs with modifications at multiple lysine sites or no modifications were removed from the global chromatin profile dataset for most analyses except the K-TSP algorithm, reducing the number of PTM features from 42 to 20 histone PTMs. In the metabolomics dataset, lipids and metabolites with signaling properties (triacylglycerides, ceramides, diacylglycerides, sphingomyelin, cholesterol esters, lysophosphatidylethanolamine, lysophosphatidylcholine, and phosphatidylcholine) were removed, resulting in 136 metabolites. For the CTRP drug area under the curve growth (AUC) data, we focused on drugs that affect histone PTMs, using the string 'histone|sirtuin|HDAC|demthylase|methyltransferase' as the filtering criteria to select drugs while filtering out drugs that affected DNA epigenetics. This reduced the number of drug features from 481 small molecules to 34 histone-modifying drugs.

Estimating pairwise associations between histone PTMs, metabolite levels, and drug AUC values using machine learning

We initially trained nine machine learning models of varying model complexity to evaluate their ability to infer the relationship between histone PTM levels, metabolite levels and drug AUC values. Specifically, we evaluated ordinary least squares, logistic regression, ridge regression, LASSO, K-Top Scoring Pairs (KTSP), decision trees, random forest, gradient boosting, and support vector machines. Based on the trade-off between model accuracy, simplicity, and interpretability, we selected LASSO and KTSP as the regression and classification algorithms used for downstream analyses. In our LASSO models, we prioritized interactions within the network using a Pearson Correlation Coefficient p-value cutoff of 0.05 and chose the strongest interactions. Finally, we performed univariate analyses using 1-feature, 2-feature, and 3-feature stepwise regression models.

We performed a Bayesian hyperparameter optimization procedure for each model with 30 sets of hyperparameters to obtain the best model that maximized the Pearson Correlation Coefficient for regression-based tasks and the Matthews Correlation Coefficient (MCC) for classification-based tasks. Overall model metrics are reported as the average value from 10-fold cross-validation.

We used the Benjamin Hochberg approach to correct for multiple hypotheses and obtain a False Discovery Rate (FDR). We decided to use a liberal FDR threshold of 0.25-0.33 for all correlation analyses to obtain a significant number of interactions for comparison with other

methods, which enabled us to aggregate the results of multiple machine learning models and infer the strongest associations.

Combining multiple machine learning models into a single meta-model

To simplify model interpretation and identify the most important metabolite-drug and metabolite-PTM associations, we consolidated our LASSO, K-TSP, and stepwise regression models to get a meta-model. Specifically, we performed an outer join multiplication operation between the LASSO and stepwise regression coefficients. Because the K-TSP algorithm calculates unique sets of coefficients for each metabolite K-mer associated with a drug or PTM value, that limited our ability to incorporate coefficients into this meta-model. To resolve this issue, we took the Matthews correlation coefficient (MCC) between the predicted and true outputs as multiplicative weights with the LASSO/Stepwise regression product across all drug/PTM values. The final product was used for all downstream analyses.

The resulting metabolite-drug and metabolite-PTM tables were still relatively high dimensional and comprised 136 metabolites. To simplify our results into a top 20 metabolite list, we took the sum of the consolidated coefficients across the drug, metabolite, and PTM dimension, which was used as our importance metric. Then, we took the top and bottom ten metabolites, resulting in a list of 20 metabolites for each association. We visualized two drugs of interest and the top/bottom 5 PTMs (for 10 PTMs).

Drug/Metabolite/PTM interaction networks

We constructed bidirectional directed networks using the LASSO regression coefficients to study histone PTM / metabolite and metabolite/drug AUC relationships. The edge color represents the sign of the regression coefficient, while the edge size represents the magnitude of the LASSO coefficients, where values larger in magnitude indicate stronger relationships. Pairwise relationships with a value of zero indicate no association. The node colors represent different network objects (histone PTMs, metabolites, and drugs), while the node size represents the absolute value of the object. We used a p-value < 0.05 and FDR < 0.25 from the Pearson Correlation Coefficients to filter out significant interactions. We used a liberal statistical threshold since we combined multiple methods to identify the most robust interactions. For LASSO networks with many nodes, we prioritized interactions that were the strongest in their respective datasets by selecting the upper and lower quartiles of the LASSO coefficients.

Nutrient/Histone PTM inhibitor sensitivity profiling

We evaluated drug/metabolite synergism and antagonism on A549 cell lines (ATCC), using our model predictions and correlation analysis as a guide to select nutrient supplementation conditions and histone PTM inhibitors. Using an automated platform, A549 was plated at a density of 200 cells per well in 384 well plates. Cells were grown in their respective media using standard cell culture conditions (37°C, 5%). The effect of small molecules was measured over an 8-point concentration range with three concentrations of metabolites (195, 625, and 2000 uM) with < 0.5% DMSO. Media was supplemented with D-Sorbitol (MilliporeSigma S1876-100G), 1-methylnicotinamide (Fisher Scientific 11-101-2274), reduced glutathione-ester (MilliporeSigma G6013-5G), kynurenic acid (MilliporeSigma K3375-250MG), DL homocysteine (MilliporeSigma H4628-1G), 5-adenosylhomocysteine (MilliporeSigma A9384-100MG), and D-pantothenic acid (MilliporeSigma P5155-100G). Cells were treated with histone deacetylase inhibitors Vorinostat (MilliporeSigma SML0061-5MG) and

histone demethylase inhibitor GSK-J4 (MilliporeSigma SML0701-5MG). We assessed cell count over 48 hours after compound/drug pairwise treatment as a surrogate for cell viability.

Drug sensitivity data processing

Cell count data (N=2 treatment replicates; N=12 control replicates) was normalized using the average DMSO and drug-only cell counts at each compound and drug concentration. Dose-response curves for each metabolite/drug pair were generated using the DMSO and drug-only normalized cell count data. To determine drug/metabolite synergy and antagonism, we calculated the cell count percentage in the drug/metabolite treatment over the drug-only condition. Each metabolite/drug pair was visualized as a dose-response matrix to visualize synergism or antagonism.

Acknowledgments

This work was supported by faculty start-up funds from the University of Michigan (UM), Camille and Henry Dreyfus Foundation, the Rogel Cancer Center at UM, R35 GM13779501 from NIH to SC, and the Proteogenomics of Cancer Training Program to SEC. We thank Peter Toogood and Andy Alt at the Michigan Drug Discovery core for discussions on the experimental assays, Madeline Shay for assistance with the experiments, Costas Lyssiotis, Yali Dou, Tim Cernak, Sriram Venneti, Max Wicha and Neil Youngson for suggestions and critical feedback on the project.

Competing interests

SC served as a consultant for Axcella Health Inc. The authors declare no other competing interests.

Supplementary Figures

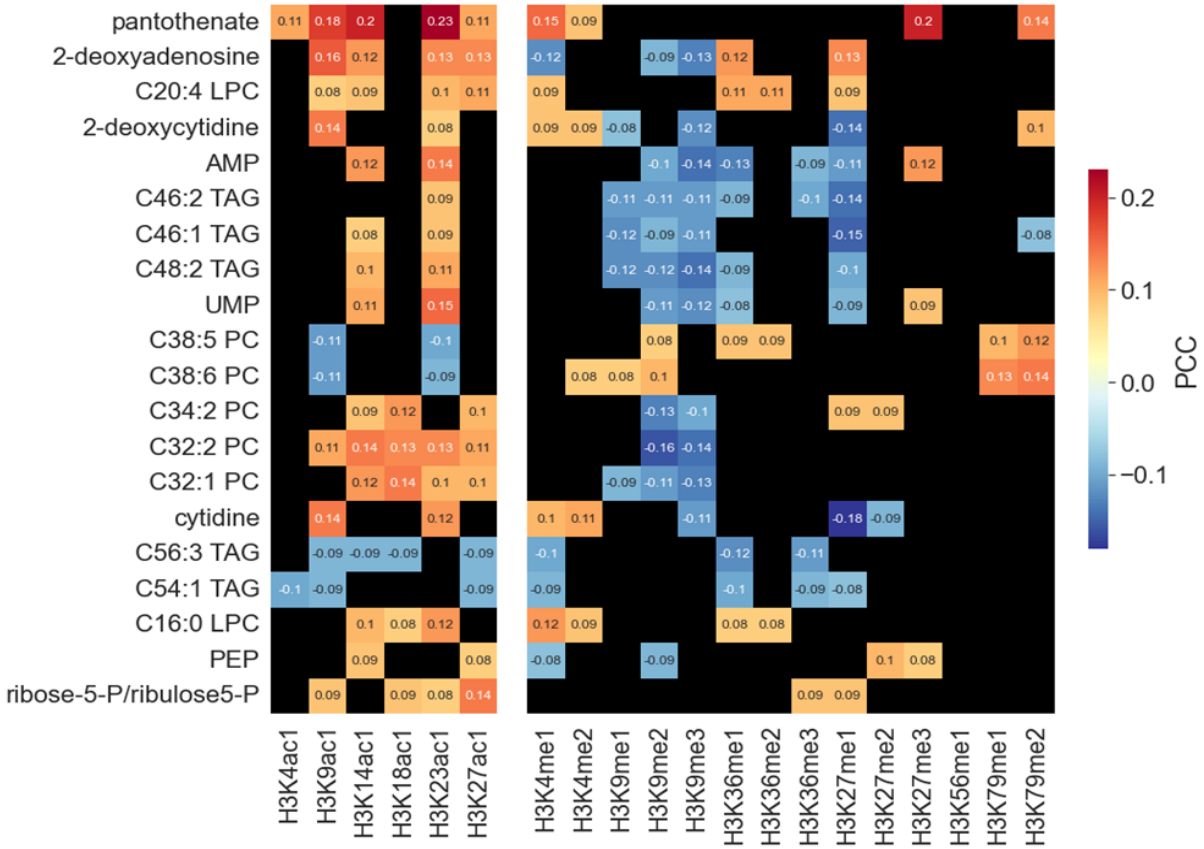

Supplementary Figure 1. correlation profiles for metabolite/PTM correlations using both metabolite and lipid data.
Histone PTM and metabolite Pearson's correlation coefficient (correlation) profile for the top 20 metabolites/lipids with the highest number of statistically significant interactions (correlation p-value < 0.05; black = non-significant). The left side of the heatmap shows histone acetylation PTMs while the right side shows histone methylation PTMs. Colors closer to red indicate a positive correlation, while blue indicates a negative correlation. TAG = Triacylglycerides. PC = Phosphatidylcholine. CE = Ceramide. LPC = Lysophosphatidylcholine. SM = Sphingomyelin.

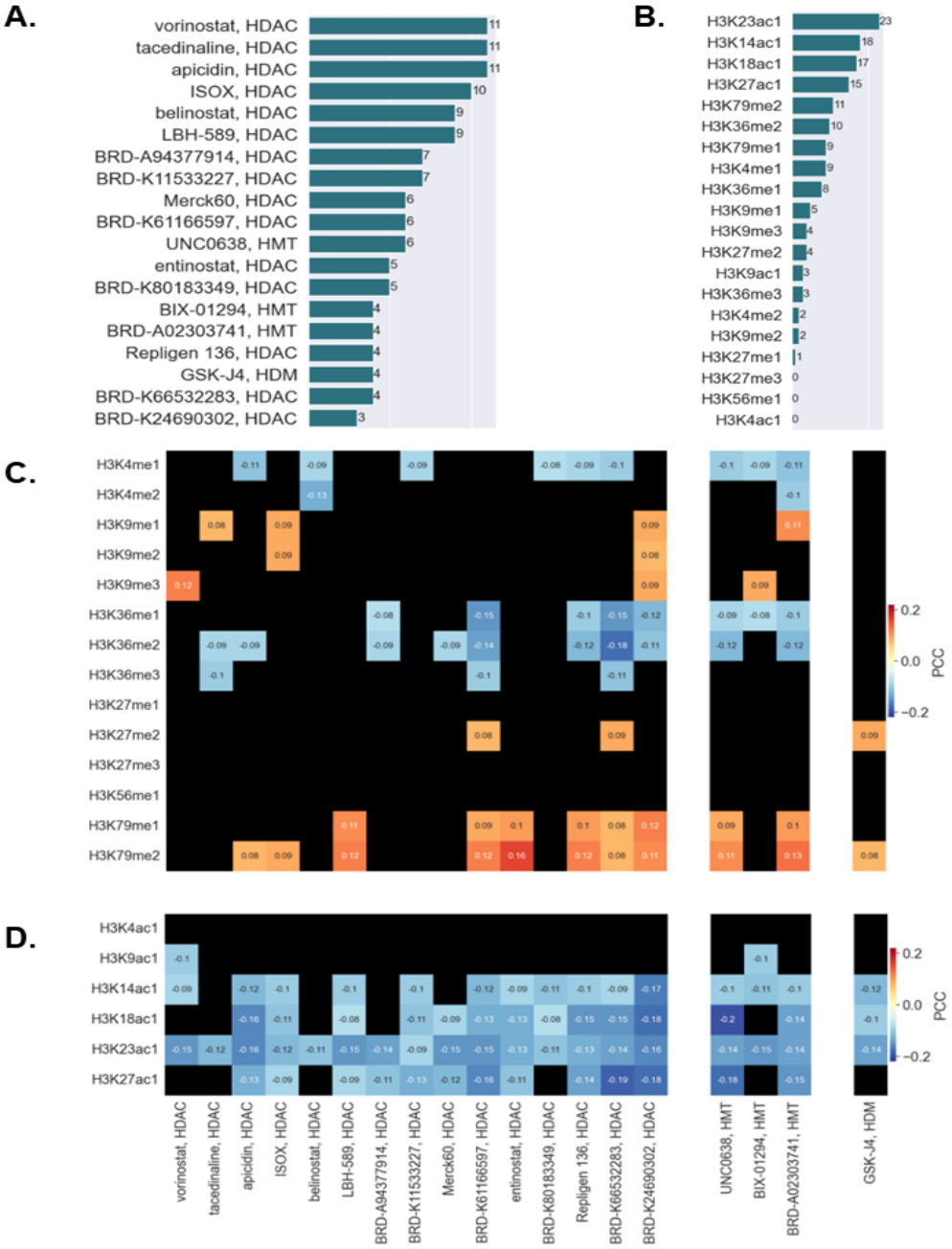

Supplementary Figure 2. Correlation profile between GCP and drug sensitivity
A) Number of statistically significant histone PTMs (x-axis) associated with a given drug (y-axis).
B) Number of statistically significant histone-modifying drugs (x-axis) associated with a given PTM (y-axis).
C) H3 methylation and their correlations between HDAC, HMT, and HDM inhibitor drug AUC values. Positive correlations with p-value < 0.05, FDR < 0.25 shown in red, while negative correlations with p-value < 0.05, FDR < 0.25 are shown in blue. Non-significant correlations are masked in black.
D) H3 acetylation and their correlations between HDAC, HMT, and HDM inhibitor drug AUC values. Positive correlations with p-value < 0.05, FDR < 0.25 shown in red, while negative correlations with p-value < 0.05, FDR < 0.25 are shown in blue. Non-significant correlations are masked in black.

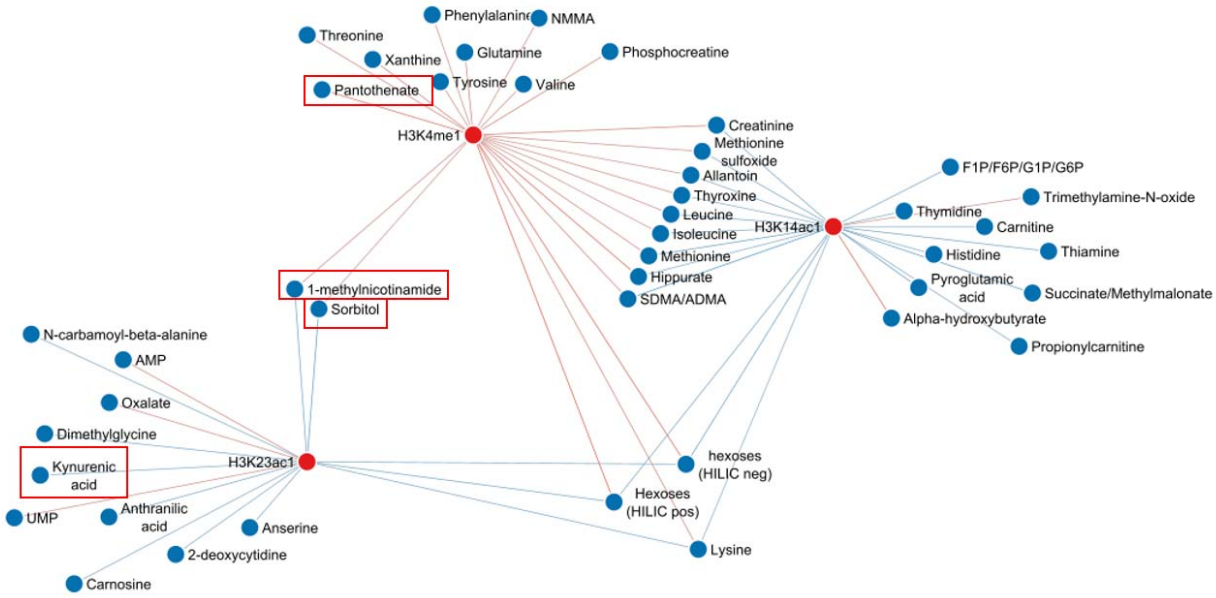

Supplementary Figure 3. LASSO metabolomics/histone PTM CCLE predictions
The top 30 metabolites with the strongest LASSO coefficients within the range of -0.15 (blue) to 0.15 (red). The metabolite/PTM interactions were filtered to have a correlation p-value < 0.05. Red nodes represent PTMs, while blue nodes represent metabolites. Red edges are positive LASSO coefficient values, while blue edges are negative coefficients. Shown in red boxes are metabolites of experimental interest based on recurrence from previous analyses or biological hypotheses.

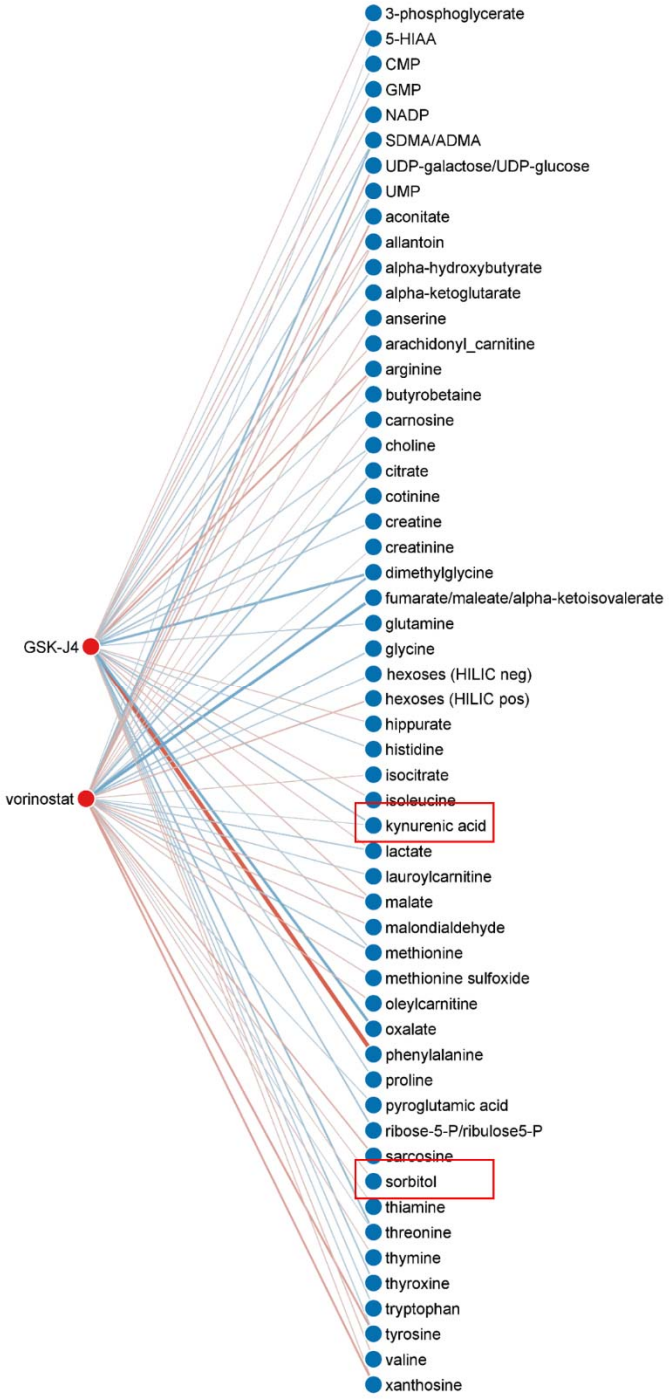

Supplementary Figure 4. LASSO histone PTM drug AUC/ metabolite CCLE predictions
Predicting drug AUC using metabolomics data. Red nodes represent drugs, while blue nodes represent metabolites. Red edges represent positive LASSO coefficients, while blue edges represent negative LASSO coefficients. The coefficient values range from 0.42 (red) to -0.39 (blue). Kynurenic acid is a metabolite of interest predicted to have a synergistic relationship with the H3K27 demethylase inhibitor GSK-J4.

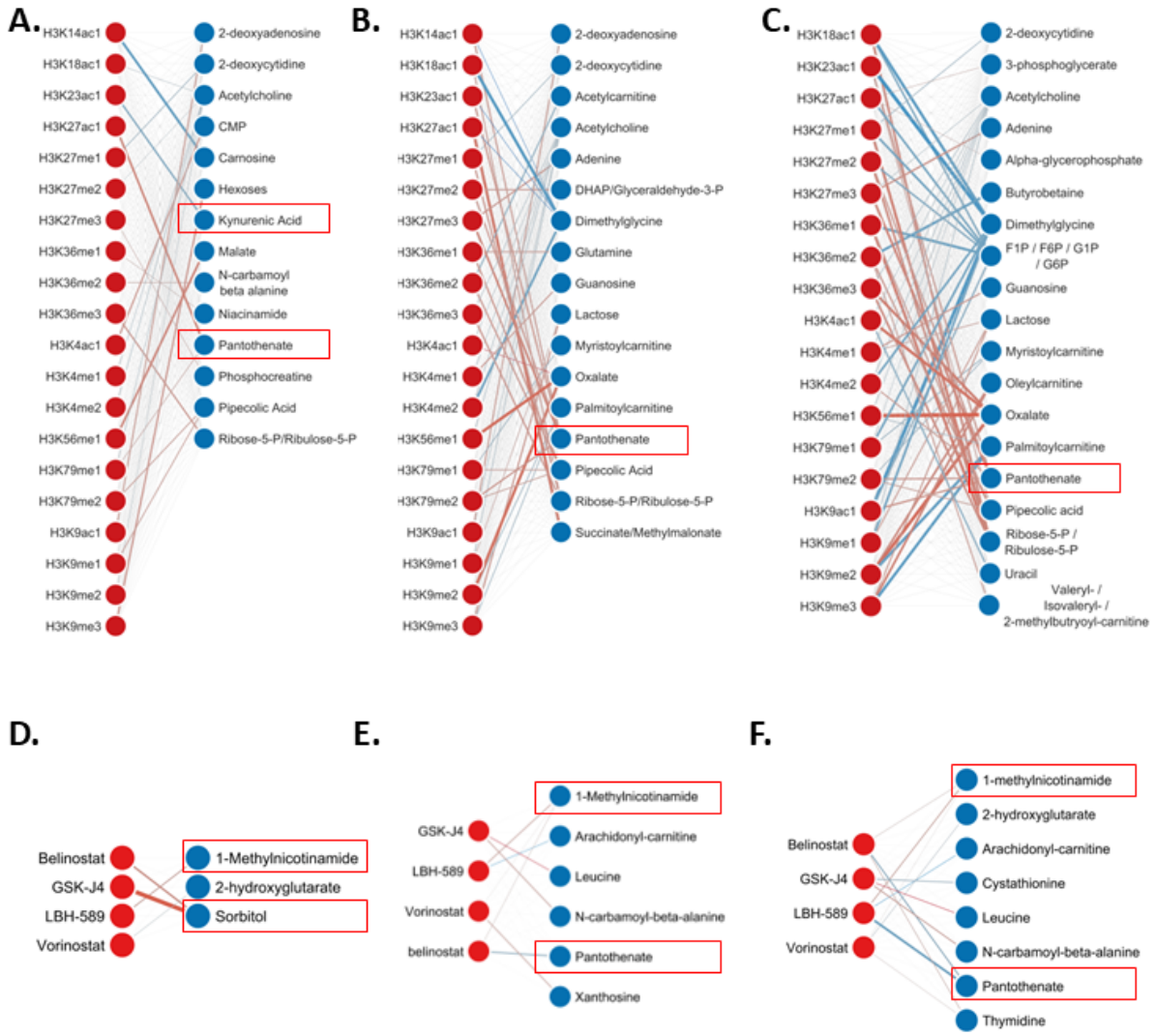

Supplementary Figure 5. Stepwise regression predictions for metabolite/PTM and metabolite/AUC interactions

A. Single metabolite PTM predictions. Red nodes represent histone PTMs. Blue nodes represent metabolites. Red edges represent positive stepwise regression coefficients, while blue edges represent negative coefficients. Thicker edges indicate strong interactions via the magnitude of the coefficient. Metabolites highlighted in red are recurring metabolites with an epigenetic interaction of interest.

B. Two metabolite PTM predictions.

C. Three metabolite PTM predictions.

D. Single metabolite drug predictions. Red nodes represent histone-modifying drugs. Blue nodes represent metabolites. Red edges represent positive stepwise regression coefficients, while blue edges represent negative coefficients. Thicker edges indicate strong interactions via the magnitude of the coefficient. Metabolites highlighted in red are recurring metabolites that have a drug-associated interaction of interest.

E. Two metabolite AUC predictions.

F. Three metabolite AUC predictions.

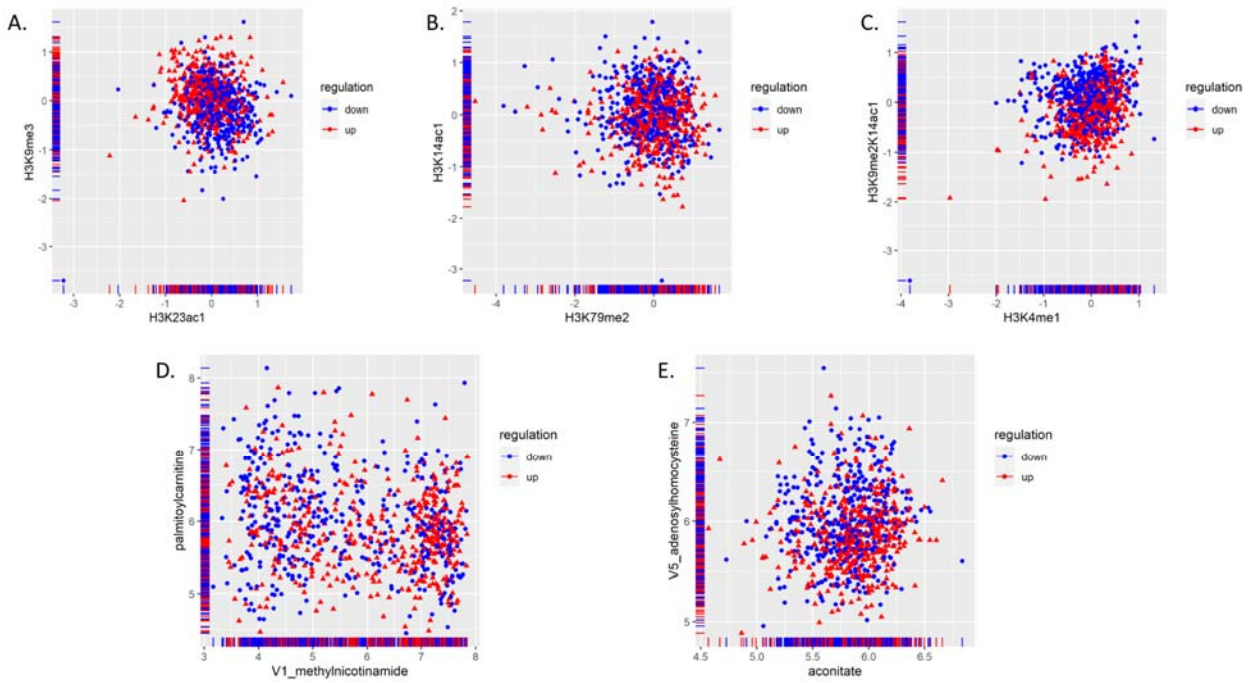

Supplementary Figure 6. 1-MNAM and H3K9me3 k-TSP predictions
A. Joint distribution between H3K23ac and H3K9me3, a PTM pair highly predictive of 1-MNAM levels. A red dot indicates that a given cell line had upregulated levels of a histone PTM while predicting 1-MNAM levels, while blue indicates downregulation.
B. H3K14ac and H3K72me2 joint distribution for predicting 1-MNAM.
C. H3K4me1 and multi-site PTM H3K9me2K14ac1 joint distribution for predicting 1-MNAM.
D. 1-MNAM and pamitolycarnitine were two metabolites that strongly predicted H3K9me3 levels. A red dot indicates that a given cell line had upregulated levels of a metabolite while predicting H3K9me levels, while blue indicates downregulation.
E. Adenosylhomocysteine and aconitate joint distribution for predicting H3K9me3.

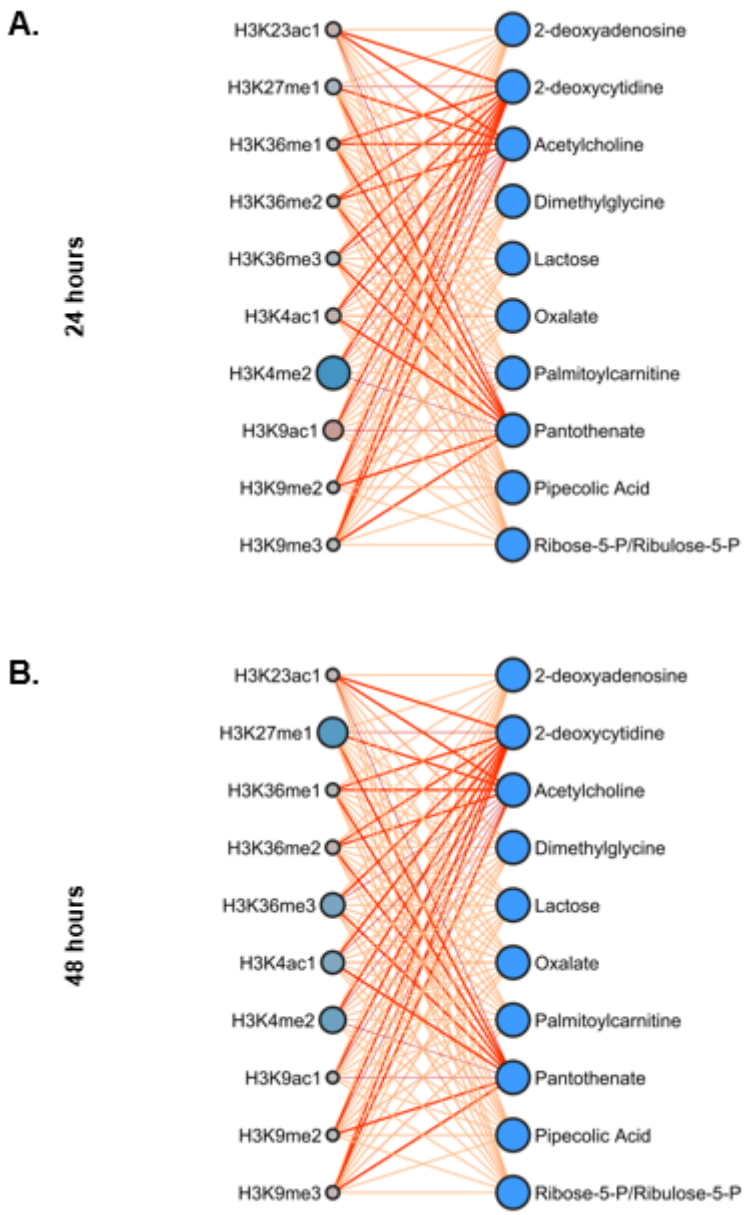

Supplementary Figure 7. Assessing the metabolic impact on histone PTM status during EMT
A. EMT time-course proteomics from Lu et al., 2019 was measured from 0-48 hours, and the Log2 Fold Change (LFC) between day X and day 0 is overlaid onto the meta-model network predictions using metabolomics to predict histone methylation and acetylation in **Figure 3**. LFC of the histone PTM levels (24 hours / 0 hour) is shown, where red is a positive LFC, gray is an LFC close to 0, and blue is a negative LFC. The size of the PTM node is the absolute value of the LFC. Many top metabolites did not intersect with the Nakasuka et al. dataset. Thus, the metabolomics LFC is not shown.
B. 48 hours histone PTM LFC overlaid onto the meta-model network.

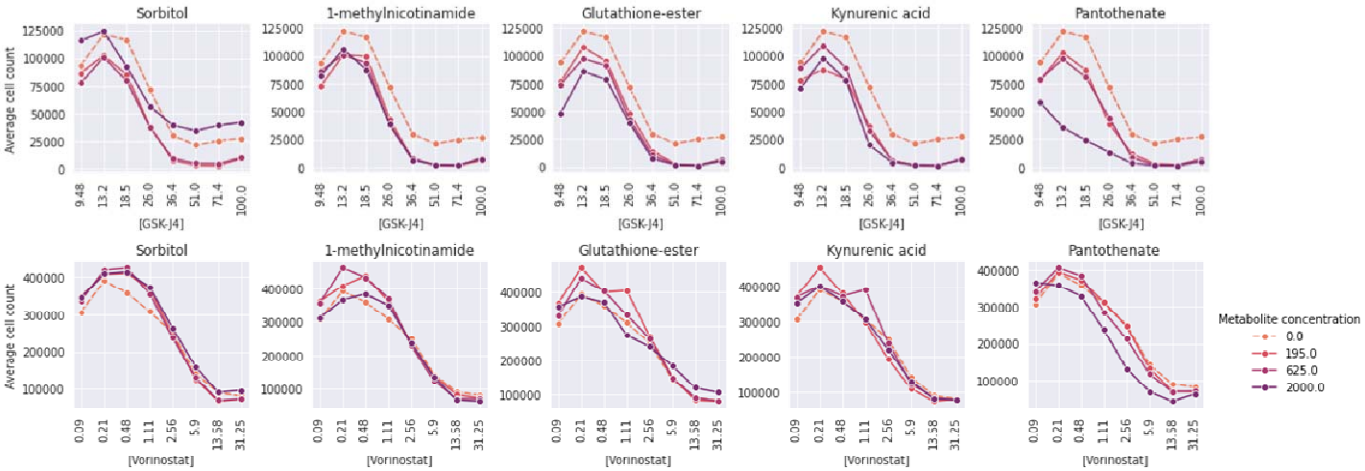

Supplementary Figure 8. Metabolite/epigenetic drug dose-response curves for A549 using DMSO reference

Normalized growth curves (treatment/control) for five metabolites + epigenetic drugs Vorinostat and GSK-J4. Control was DMSO/water condition. The black line indicates no difference between treatment and control. Data points were averaged across replicates (N=2 treatment replicates; N=12 control replicates).

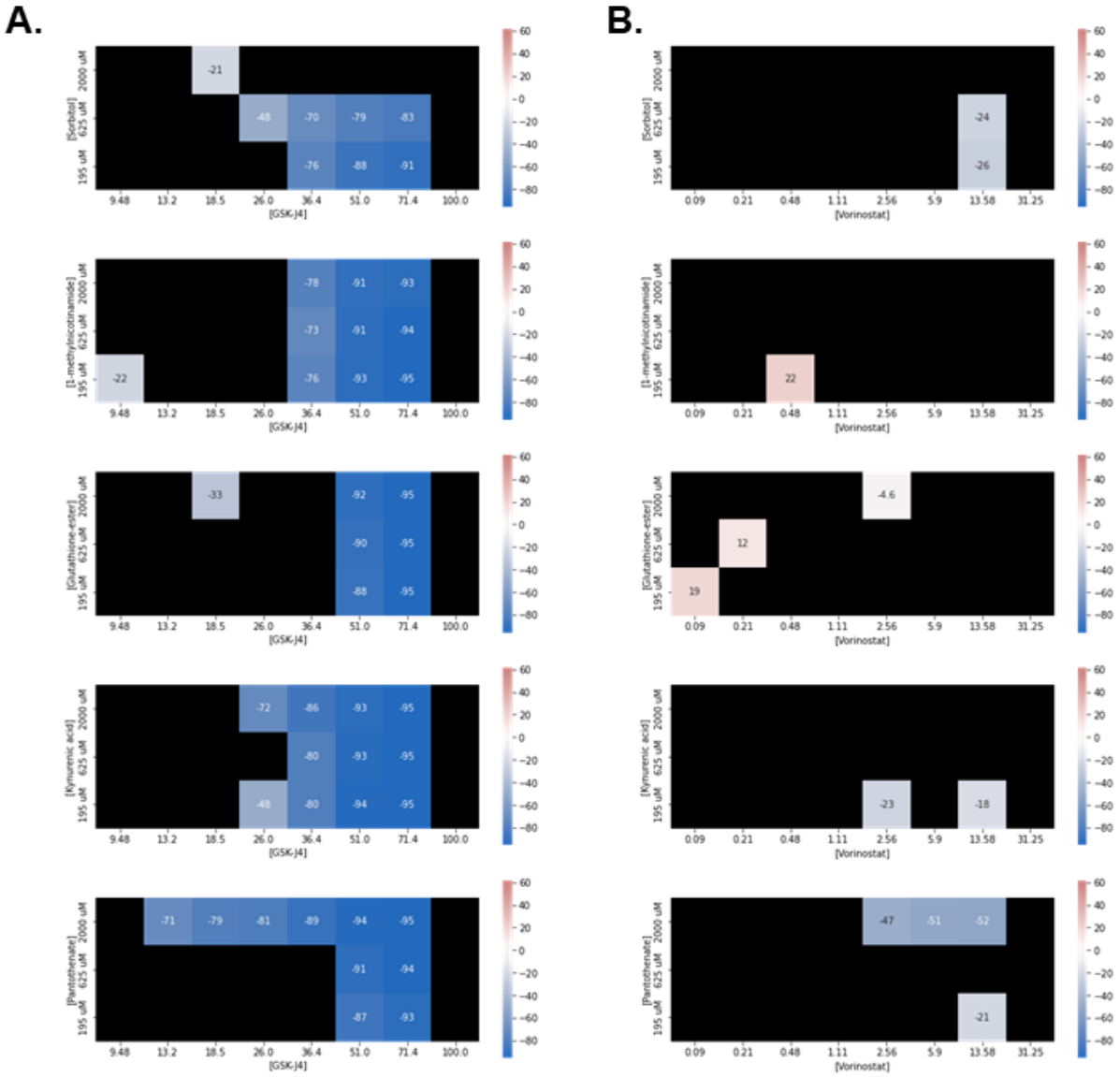

Supplementary Figure 9. Metabolite/drug 2D dose-response profiles for Vorinostat and GSK-J4 in A549

A. Significant metabolite/drug interactions (T-test; p-value < 0.05) between GSK-J4 and five other metabolites identified from our analyses. The percent changes in cell count between treatment (GSK-J4/Metabolite) and control (DMSO/Water) are shown. Red cells indicate increased cell viability with drug/metabolite treatment, while blue cells indicate decreased cell viability for the control.

B. Significant interactions between Vorinostat and metabolites.

Supplementary Methods

Predicting multi-variate histone PTM/metabolite interactions using KTSP

We trained K-Top Scoring Pairs (KTSP) models (Yoon & Kim, 2010), which inherently perform dimensionality reduction to select the top pairs of histone PTMs predictive of metabolite levels and vice-versa. KTSP classifiers were trained on histone PTM data to predict metabolite regulation, using the threshold of 0 to label the metabolite or histone PTM classified as upregulated (positive values) or downregulated (negative values). We utilized all 42 histone PTMs to capture multi-site relationships in this instance. Histone PTM status was used as a feature in the model, and the description of the four histone PTM status categories are below:

- **No methylation:** PTMs with no methylation groups present in them
- **Methylation:** PTMs with one or more methylation modifications present in them. Acetylation modifications can also be present for multi-site PTMs.
- **No acetylation:** PTMs with no acetylation present
- **Acetylation:** PTMs with one or more acetylation modifications. Methyl modifications can also be present for multi-site PTMs.

We performed additional feature engineering, including the sum and variance of histone PTM levels and the cell line growth doubling time to evaluate the impact of these features on metabolite or histone PTM levels. We trained k-TSP models on 51 histone PTM features and 136 non-lipid and non-signaling metabolites.

K-Top Scoring Pairs Calculations

An example of our implementation of the k-TSP algorithm is shown below:

For PTM pair P_A, P_B:

$Score_{PA\text{-}PB}(metabolite) = abs\ (T_{PA\text{-}PB}(1) - T_{PA\text{-}PB}(0))$, where
$T_{PA\text{-}PB}(1) = Pr(P_A < P_B |\ label = 1)$ and $T_{PA\text{-}PB}(0) = Pr(P_A < P_B |\ label = 0)$

The calculation of score between PTM pair H3K4me1 and H3K9me2K14ac1 for 1-methylnicotinamide is shown below:
Let H3K4me1 be P_A and H3K9me2K14ac1 be P_B
$T_{PA\text{-}PB}(0) = Pr(P_A < P_B \mid y=0)$
= number of subjects that have $P_A < P_B$ with label 0 / total number of subjects with label 0
= 321/523
= 0.614

$T_{PA\text{-}PB}(1) = Pr(P_A < P_B \mid y=1)$
= number of subjects that have $P_A < P_B$ with label 1 / total number of subjects with label 1
= 115/356
= 0.323

$$S_{PA\text{-}PB}(\text{1-methylnicotinamide}) = \text{abs}(T_{PA\text{-}PB}(1) - T_{PA\text{-}PB}(0))$$
$$= \text{abs}\ (0.323 - 0.614)$$
$$= 0.29$$

Supplementary Tables

S. Table 1 Pearson correlation coefficients between metabolite/PTM interactions
S. Table 2 Literature validation of metabolite/histone PTM interactions
S. Table 3 Pearson correlation coefficients between metabolites and drug sensitivity data

S. Table 4 Pearson correlation coefficients between drug sensitivity data and histone PTM levels
S. Table 5 LASSO Met/PTM interactions
S. Table 6 LASSO Met/AUC interactions
S. Table 7 Stepwise regression interactions
S. Table 8 Aggregated ML metabolite/PTM model (top 20 metabolites)
S. Table 9 Aggregated ML metabolite/Drug model (top 20 metabolites)
S. Table 10 Summary of metabolite/PTM interactions predicted by correlations and ML
S. Table 11 Summary of metabolite/drug interactions predicted by correlations and ML

References

1. Chen, C., Wang, Z. & Qin, Y. Connections between metabolism and epigenetics: mechanisms and novel anti-cancer strategy. *Front Pharmacol* **13**, 935536 (2022).
2. Kaelin, W.G., Jr. & McKnight, S.L. Influence of metabolism on epigenetics and disease. *Cell* **153**, 56-69 (2013).
3. Reid, M.A., Dai, Z. & Locasale, J.W. The impact of cellular metabolism on chromatin dynamics and epigenetics. *Nat Cell Biol* **19**, 1298-1306 (2017).
4. Su, X., Wellen, K.E. & Rabinowitz, J.D. Metabolic control of methylation and acetylation. *Curr Opin Chem Biol* **30**, 52-60 (2016).
5. Cai, L., Sutter, B.M., Li, B. & Tu, B.P. Acetyl-CoA induces cell growth and proliferation by promoting the acetylation of histones at growth genes. *Mol Cell* **42**, 426-437 (2011).
6. Gao, X. et al. Acetate functions as an epigenetic metabolite to promote lipid synthesis under hypoxia. *Nature Communications* **7**, 11960 (2016).
7. Gallinari, P., Marco, S.D., Jones, P., Pallaoro, M. & Steinkühler, C. HDACs, histone deacetylation and gene transcription: from molecular biology to cancer therapeutics. *Cell Research* **17**, 195-211 (2007).
8. Locasale, J.W. Serine, glycine and one-carbon units: cancer metabolism in full circle. *Nat Rev Cancer* **13**, 572-583 (2013).
9. Newman, A.C. & Maddocks, O.D.K. One-carbon metabolism in cancer. *British Journal of Cancer* **116**, 1499-1504 (2017).
10. Black, J.C., Van Rechem, C. & Whetstine, J.R. Histone lysine methylation dynamics: establishment, regulation, and biological impact. *Mol Cell* **48**, 491-507 (2012).
11. Hyun, K., Jeon, J., Park, K. & Kim, J. Writing, erasing and reading histone lysine methylations. *Experimental & Molecular Medicine* **49**, e324-e324 (2017).
12. Campit, S.E., Meliki, A., Youngson, N.A. & Chandrasekaran, S. Nutrient Sensing by Histone Marks: Reading the Metabolic Histone Code Using Tracing, Omics, and Modeling. *BioEssays* **42**, 2000083 (2020).
13. Tu, B.P., Kudlicki, A., Rowicka, M. & McKnight, S.L. Logic of the yeast metabolic cycle: temporal compartmentalization of cellular processes. *Science* **310**, 1152-1158 (2005).
14. Tran, T.Q., Lowman, X.H. & Kong, M. Molecular Pathways: Metabolic Control of Histone Methylation and Gene Expression in Cancer. *Clin Cancer Res* **23**, 4004-4009 (2017).
15. Morrish, F. et al. Myc-dependent mitochondrial generation of acetyl-CoA contributes to fatty acid biosynthesis and histone acetylation during cell cycle entry. *J Biol Chem* **285**, 36267-36274 (2010).
16. Lee, J.V. et al. Akt-dependent metabolic reprogramming regulates tumor cell histone acetylation. *Cell Metab* **20**, 306-319 (2014).
17. Solary, E., Bernard, O.A., Tefferi, A., Fuks, F. & Vainchenker, W. The Ten-Eleven Translocation-2 (TET2) gene in hematopoiesis and hematopoietic diseases. *Leukemia* **28**, 485-496 (2014).
18. Sciacovelli, M. et al. Fumarate is an epigenetic modifier that elicits epithelial-to-mesenchymal transition. *Nature* **537**, 544-547 (2016).
19. Pavlova, N.N. & Thompson, C.B. The Emerging Hallmarks of Cancer Metabolism. *Cell Metab* **23**, 27-47 (2016).
20. Kinnaird, A., Zhao, S., Wellen, K.E. & Michelakis, E.D. Metabolic control of epigenetics in cancer. *Nat Rev Cancer* **16**, 694-707 (2016).
21. DeBerardinis, R.J. & Chandel, N.S. Fundamentals of cancer metabolism. *Sci Adv* **2**, e1600200 (2016).
22. Vogelstein, B. et al. Cancer genome landscapes. *Science* **339**, 1546-1558 (2013).

23. Seth Nanda, C., Venkateswaran, S.V., Patani, N. & Yuneva, M. Defining a metabolic landscape of tumours: genome meets metabolism. *British Journal of Cancer* **122**, 136-149 (2020).
24. Cheng, Y. et al. Targeting epigenetic regulators for cancer therapy: mechanisms and advances in clinical trials. *Signal Transduction and Targeted Therapy* **4**, 62 (2019).
25. King, J., Patel, M. & Chandrasekaran, S. Metabolism, HDACs, and HDAC Inhibitors: A Systems Biology Perspective. *Metabolites* **11** (2021).
26. Mann, B.S., Johnson, J.R., Cohen, M.H., Justice, R. & Pazdur, R. FDA approval summary: vorinostat for treatment of advanced primary cutaneous T-cell lymphoma. *Oncologist* **12**, 1247-1252 (2007).
27. Ganesan, A., Arimondo, P.B., Rots, M.G., Jeronimo, C. & Berdasco, M. The timeline of epigenetic drug discovery: from reality to dreams. *Clinical Epigenetics* **11**, 174 (2019).
28. Shen, F., Boccuto, L., Pauly, R., Srikanth, S. & Chandrasekaran, S. Genome-scale network model of metabolism and histone acetylation reveals metabolic dependencies of histone deacetylase inhibitors. *Genome Biology* **20**, 49 (2019).
29. Joly, J.H., Chew, B.T.L. & Graham, N.A. The landscape of metabolic pathway dependencies in cancer cell lines. *PLOS Computational Biology* **17**, e1008942 (2021).
30. Li, H. et al. The landscape of cancer cell line metabolism. *Nature Medicine* **25**, 850-860 (2019).
31. Ghandi, M. et al. Next-generation characterization of the Cancer Cell Line Encyclopedia. *Nature* **569**, 503-508 (2019).
32. Suganuma, T. & Workman, J.L. Nucleotide Metabolism Behind Epigenetics. *Frontiers in Endocrinology* **12** (2021).
33. Wang, W., Yang, C., Wang, T. & Deng, H. Complex roles of nicotinamide N-methyltransferase in cancer progression. *Cell Death & Disease* **13**, 267 (2022).
34. Kraus, D. et al. Nicotinamide N-methyltransferase knockdown protects against diet-induced obesity. *Nature* **508**, 258-262 (2014).
35. Zhang, J., Chen, Y., Liu, C., Li, L. & Li, P. N(1)-Methylnicotinamide Improves Hepatic Insulin Sensitivity via Activation of SIRT1 and Inhibition of FOXO1 Acetylation. *J Diabetes Res* **2020**, 1080152 (2020).
36. Koutsioumpa, M. et al. Lysine methyltransferase 2D regulates pancreatic carcinogenesis through metabolic reprogramming. *Gut* **68**, 1271-1286 (2019).
37. Klein, B.J. et al. Histone H3K23-specific acetylation by MORF is coupled to H3K14 acylation. *Nature Communications* **10**, 4724 (2019).
38. Audia, J.E. & Campbell, R.M. Histone Modifications and Cancer. *Cold Spring Harb Perspect Biol* **8**, a019521 (2016).
39. Pilz, R.B., Willis, R.C. & Boss, G.R. The influence of ribose 5-phosphate availability on purine synthesis of cultured human lymphoblasts and mitogen-stimulated lymphocytes. *J Biol Chem* **259**, 2927-2935 (1984).
40. Kee, J. et al. SARS-CoV-2 disrupts host epigenetic regulation via histone mimicry. *Nature* **610**, 381-388 (2022).
41. Zhao, Y. & Garcia, B.A. Comprehensive Catalog of Currently Documented Histone Modifications. *Cold Spring Harb Perspect Biol* **7**, a025064 (2015).
42. Seashore-Ludlow, B. et al. Harnessing Connectivity in a Large-Scale Small-Molecule Sensitivity Dataset. *Cancer Discov* **5**, 1210-1223 (2015).
43. Traverso, N. et al. Role of glutathione in cancer progression and chemoresistance. *Oxid Med Cell Longev* **2013**, 972913 (2013).
44. García-Giménez, J.L. & Pallardó, F.V. Maintenance of glutathione levels and its importance in epigenetic regulation. *Front Pharmacol* **5**, 88 (2014).

45. Shen, Y. et al. Activation of the Jnk signaling pathway by a dual-specificity phosphatase, JSP-1. *Proceedings of the National Academy of Sciences* **98**, 13613-13618 (2001).
46. Roberti, A., Fernández, A.F. & Fraga, M.F. Nicotinamide N-methyltransferase: At the crossroads between cellular metabolism and epigenetic regulation. *Molecular Metabolism* **45**, 101165 (2021).
47. Sebastián, C. & Mostoslavsky, R. The Various Metabolic Sources of Histone Acetylation. *Trends Endocrinol Metab* **28**, 85-87 (2017).
48. Walczak, K., Wnorowski, A., Turski, W.A. & Plech, T. Kynurenic acid and cancer: facts and controversies. *Cell Mol Life Sci* **77**, 1531-1550 (2020).
49. Szabo, M. et al. Kynurenic Acid and Its Analog SZR104 Exhibit Strong Antiinflammatory Effects and Alter the Intracellular Distribution and Methylation Patterns of H3 Histones in Immunochallenged Microglia-Enriched Cultures of Newborn Rat Brains. *Int J Mol Sci* **23** (2022).
50. Srinivasan, B. & Sibon, O.C. Coenzyme A, more than 'just' a metabolic cofactor. *Biochem Soc Trans* **42**, 1075-1079 (2014).
51. Xu, W.S., Parmigiani, R.B. & Marks, P.A. Histone deacetylase inhibitors: molecular mechanisms of action. *Oncogene* **26**, 5541-5552 (2007).
52. Kruidenier, L. et al. A selective jumonji H3K27 demethylase inhibitor modulates the proinflammatory macrophage response. *Nature* **488**, 404-408 (2012).
53. Ghasemi, S. Cancer's epigenetic drugs: where are they in the cancer medicines? *The Pharmacogenomics Journal* **20**, 367-379 (2020).
54. Hong, S. et al. Nicotinamide N-methyltransferase regulates hepatic nutrient metabolism through Sirt1 protein stabilization. *Nat Med* **21**, 887-894 (2015).
55. Bakir, B., Chiarella, A.M., Pitarresi, J.R. & Rustgi, A.K. EMT, MET, Plasticity, and Tumor Metastasis. *Trends in Cell Biology* **30**, 764-776 (2020).
56. Huang, Y., Hong, W. & Wei, X. The molecular mechanisms and therapeutic strategies of EMT in tumor progression and metastasis. *Journal of Hematology & Oncology* **15**, 129 (2022).
57. Nakasuka, F. et al. TGF-β-dependent reprogramming of amino acid metabolism induces epithelial–mesenchymal transition in non-small cell lung cancers. *Communications Biology* **4**, 782 (2021).
58. Lu, C. et al. Coordination between TGF-β cellular signaling and epigenetic regulation during epithelial to mesenchymal transition. *Epigenetics Chromatin* **12**, 11 (2019).
59. Campit, S., Keshamouni, V.G. & Chandrasekaran, S. Constraint-based modeling identifies metabolic vulnerabilities during the epithelial to mesenchymal transition. *bioRxiv*, 2022.2001.2031.478483 (2022).
60. Funasaka, T., Hogan, V. & Raz, A. Phosphoglucose isomerase/autocrine motility factor mediates epithelial and mesenchymal phenotype conversions in breast cancer. *Cancer Res* **69**, 5349-5356 (2009).
61. Zhang, D. et al. High glucose induces the aging of mesenchymal stem cells via Akt/mTOR signaling. *Mol Med Rep* **16**, 1685-1690 (2017).
62. Tang, H.M. et al. An epithelial marker promoter induction screen identifies histone deacetylase inhibitors to restore epithelial differentiation and abolishes anchorage independence growth in cancers. *Cell Death Discovery* **2**, 16041 (2016).
63. Sakamoto, T. et al. A Histone Deacetylase Inhibitor Suppresses Epithelial-Mesenchymal Transition and Attenuates Chemoresistance in Biliary Tract Cancer. *PLoS One* **11**, e0145985 (2016).
64. Gao, X. et al. Dietary methionine influences therapy in mouse cancer models and alters human metabolism. *Nature* **572**, 397-401 (2019).

65. Miyamoto, K. et al. xCT Inhibition Increases Sensitivity to Vorinostat in a ROS-Dependent Manner. *Cancers (Basel)* **12** (2020).
66. Miermont, A. et al. Severe osmotic compression triggers a slowdown of intracellular signaling, which can be explained by molecular crowding. *Proc Natl Acad Sci U S A* **110**, 5725-5730 (2013).
67. Zhang, T., Gong, Y., Meng, H., Li, C. & Xue, L. Symphony of epigenetic and metabolic regulation—interaction between the histone methyltransferase EZH2 and metabolism of tumor. *Clinical Epigenetics* **12**, 72 (2020).
68. Hashizume, R. et al. Pharmacologic inhibition of histone demethylation as a therapy for pediatric brainstem glioma. *Nature Medicine* **20**, 1394-1396 (2014).
69. Adams, S. et al. Involvement of the kynurenine pathway in human glioma pathophysiology. *PLoS One* **9**, e112945 (2014).
70. Platten, M., Nollen, E.A.A., Röhrig, U.F., Fallarino, F. & Opitz, C.A. Tryptophan metabolism as a common therapeutic target in cancer, neurodegeneration and beyond. *Nature Reviews Drug Discovery* **18**, 379-401 (2019).
71. Chung, C. et al. Integrated Metabolic and Epigenomic Reprograming by H3K27M Mutations in Diffuse Intrinsic Pontine Gliomas. *Cancer Cell* **38**, 334-349.e339 (2020).
72. Vaissière, T., Sawan, C. & Herceg, Z. Epigenetic interplay between histone modifications and DNA methylation in gene silencing. *Mutation Research/Reviews in Mutation Research* **659**, 40-48 (2008).
73. Zhang, B. et al. Crosstalk between DNA methylation and histone acetylation triggers GDNF high transcription in glioblastoma cells. *Clinical Epigenetics* **12**, 47 (2020).
74. Dang, L. et al. Cancer-associated IDH1 mutations produce 2-hydroxyglutarate. *Nature* **462**, 739-744 (2009).
75. Xu, W. et al. Oncometabolite 2-hydroxyglutarate is a competitive inhibitor of α-ketoglutarate-dependent dioxygenases. *Cancer Cell* **19**, 17-30 (2011).
76. Dow, J. et al. Vulnerability of IDH1-Mutant Cancers to Histone Deacetylase Inhibition via Orthogonal Suppression of DNA Repair. *Molecular Cancer Research* **19**, 2057-2067 (2021).
77. Munn, D.H. & Mellor, A.L. IDO in the Tumor Microenvironment: Inflammation, Counter-Regulation, and Tolerance. *Trends Immunol* **37**, 193-207 (2016).
78. Fontebasso, A.M., Liu, X.Y., Sturm, D. & Jabado, N. Chromatin remodeling defects in pediatric and young adult glioblastoma: a tale of a variant histone 3 tail. *Brain Pathol* **23**, 210-216 (2013).
79. Schwartzentruber, J. et al. Driver mutations in histone H3.3 and chromatin remodelling genes in paediatric glioblastoma. *Nature* **482**, 226-231 (2012).
80. Lin, Z. & Fang, D. The Roles of SIRT1 in Cancer. *Genes Cancer* **4**, 97-104 (2013).
81. An, Y. et al. SIRT1 inhibits chemoresistance and cancer stemness of gastric cancer by initiating an AMPK/FOXO3 positive feedback loop. *Cell Death & Disease* **11**, 115 (2020).
82. Kilgour, M.K. et al. 1-Methylnicotinamide is an immune regulatory metabolite in human ovarian cancer. *Sci Adv* **7** (2021).
83. Gebicki, J. & Wieczorkowska, M. COVID-19 infection: mitohormetic concept of immune response. *Cell Death Discovery* **6**, 60 (2020).
84. Mau, T. & Yung, R. Potential of epigenetic therapies in non-cancerous conditions. *Frontiers in Genetics* **5** (2014).
85. Tzika, E., Dreker, T. & Imhof, A. Epigenetics and Metabolism in Health and Disease. *Frontiers in Genetics* **9** (2018).
86. Lyssiotis, C.A. & Kimmelman, A.C. Metabolic Interactions in the Tumor Microenvironment. *Trends in Cell Biology* **27**, 863-875 (2017).

87. Jin, M.-Z. & Jin, W.-L. The updated landscape of tumor microenvironment and drug repurposing. *Signal Transduction and Targeted Therapy* **5**, 166 (2020).
88. Mittal, A. et al. Radiotherapy-induced metabolic hallmarks in the tumor microenvironment. *Trends in Cancer* **8**, 855-869 (2022).